January 2017

Predicting Response To Anti-Pd-1 Immunotherapy In Metastatic Melanoma

James William Smithy

Yale University, jwsmithy@gmail.com

Follow this and additional works at: http://elischolar.library.yale.edu/ymtdl

Predicting Response to Anti-PD-1 Immunotherapy in Metastatic Melanoma

A Thesis Submitted to the
Yale University School of Medicine
in Partial Fulfillment of the Requirements for the
Degree of Doctor of Medicine

by
James William Smithy
2017

ABSTRACT

PREDICTING RESPONSE TO ANTI-PD-1 IMMUNOTHERAPY IN METASTATIC MELANOMA

James W. Smithy,[1] Lauren M. Moore,[1] Kim Blenman,[2] Vasiliki Pelekanou,[1] Jamaal Rehman,[1] Patricia Gaule,[1] Pok Fai Wong,[1] Veronique M. Neumeister,[1] Katerina Politi,[1] Harriet M. Kluger,[3] David L. Rimm[1,3]

1. Department of Pathology, Yale School of Medicine, New Haven, CT
2. Department of Dermatology, Yale School of Medicine, New Haven, CT
3. Section of Medical Oncology, Yale School of Medicine, New Haven, CT

Predictive biomarkers for antibodies against programmed death 1 (PD-1) remain a major unmet need in metastatic melanoma. Thus, we evaluated three alternative tissue- and blood based markers biomarkers for response to anti-PD-1 therapy. First, pre-treatment melanoma samples were assayed for expression of: 1) IRF-1, a PD-L1 transcription factor, as a proxy for a tumor's capacity to express PD-L1, and 2) an immune activation panel consisting of CD3, Ki67, and Granzyme B to distinguish immune-active and immune-quiescent tumors. Additionally, we conducted pilot studies to determine the feasibility of measuring soluble PD-L1 in the plasma of cancer patients.

For tissue-based assays, samples from melanoma patients that received nivolumab, pembrolizumab, or combination ipilimumab/nivolumab at Yale New Haven Hospital from May 2013 to March 2016 were collected. Expression of IRF-1 and PD-L1 in archival pre-treatment formalin-fixed, paraffin-embedded tumor samples were assessed by the AQUA method of quantitative immunofluorescence. Objective radiographic response (ORR) and progression-free survival (PFS) were assessed using modified RECIST v1.1 criteria. For pilot studies of sPD-L1, plasma from 62 patients with

non-small cell lung cancer and 10 cancer-free controls were accessed from pre-existing de-identified tissue banks at Yale School of Medicine.

Nuclear IRF-1 expression was higher in patients with partial or complete response (PR/CR) than in patients with stable or progressive disease (SD/PD) ($p = 0.044$). There was an insignificant trend toward higher PD-L1 expression in patients with PR/CR ($p = 0.085$). PFS was higher in the IRF-1-high group than the IRF-1-low group ($p = 0.017$), while PD-L1 expression had no effect on PFS ($p = 0.83$). In a subset analysis, a strong association between IRF-1 and PFS is seen in patients treated with combination ipilimumab and nivolumab ($p = 0.0051$). Higher CD3 infiltrates were more likely to be associated with PR/CR ($p = 0.0067$) and with improved PFS ($p = 0.017$). Conversely, higher expression of Granzyme B within CD3+ cells was associated with SD/PD ($p = 0.023$) and a trend toward inferior PFS ($p = 0.066$). Soluble PD-L1 in human plasma was detected by ELISA, and was elevated in NSCLC cases compared to controls ($p < 0.0001$).

As a measure of PD-L1 expression capability, IRF-1 expression may be a more valuable predictive biomarker for anti-PD-1 therapy than PD-L1 itself. Additionally, patients with quiescent immune infiltrates may benefit more from anti-PD-1 therapy than those with immune-active tumors. The viability of plasma-based predictive biomarkers for immunotherapies warrants additional investigation.

ACKNOWLEDGEMENTS

TABLE OF CONTENTS

I. INTRODUCTION

Immune checkpoint blockade in metastatic melanoma

Evasion of host immune responses has been described as a key survival mechanism in cancer.[1] Therapeutic blockade of immune checkpoints has recently revolutionized the treatment of multiple advanced tumor types, perhaps most dramatically metastatic melanoma.

The promise of this modality in melanoma was first demonstrated by targeting the prototypical immune checkpoint molecule, cytotoxic T-lymphocyte-associated protein 4 (CTLA-4). In brief, CTLA-4 acts as an inhibitory counterpoint to the co-stimulatory receptor CD28 in the priming of naive T cells.[2] When a T cell expressing CTLA-4 encounters antigen-presenting cells, CTLA-4 competes with CD28 for its ligands, CD80 (B7-1) and CD86 (B7-2). Instead of triggering kinase cascades typical of T cell activation, CTLA-4 activation initiates an inhibitory downstream program mediated by phosphatases SHP2 and PP2A.[3] Thus, the T cell is then unable to traffic to tumors and initiate an effective anti-tumor response. As CTLA-4 has a higher affinity for CD80 and CD86 than does CD28,[4] an inhibited phenotype takes precedence when both co-receptors are present.

The clinical relevance of this pathway was demonstrated in a 2010 landmark phase III trial of the CTLA-4 blocking antibody ipilimumab.[5] This trial of 676 patients showed an objective tumor response rate of 10% of patients, and a 26% three-year survival rate in a patient population with previously dismal outcomes. So-called "durable responses" in a subset of patients have been a unique characteristic of immunotherapies,

representing a paradigm shift from cytotoxic chemotherapy and molecularly targeted therapies.

The next iteration of immune checkpoint blockade came with the development of agents targeting the axis of programmed death-1 (PD-1) and its ligand, programmed death-ligand 1 (PD-L1). Like CTLA-4, PD-1 is also an inhibitory receptor expressed on T cells. However, it acts at a later step in the tumor immunity cycle—at the point at which primed T cells would exert their cytolytic effect against tumor cells. The ligand PD-L1 is expressed on tumors as well as on antigen-presenting cells and lymphocytes in the tumor microenvironment,[6] and upon binding to PD-1, can convert cytotoxic T cells to an anergic or apoptotic state.[7] It can also reduce proliferation of T cells[8] and convert T_H1 cells to a T_{reg} phenotype.[9] In non-neoplastic contexts, this mechanism is used physiologically in pregnancy to promote fetomaternal tolerance in placenta,[10] and to protect surrounding tissue from an immune response against chronic infections.[11]

Nivolumab and pembrolizumab are two monoclonal antibodies against PD-1, and were first investigated as monotherapies across a number of tumor types.[12] Given the promising response rates in melanoma, larger-scale trials were quickly initiated for this indication. In the phase III CheckMate 066 trial, nivolumab showed an objective response rate of 40%, with a median progression-free response rate of 5.1 months.[13] Grade 3 or 4 adverse events were relatively infrequent, observed in 11.7% of patients. The response rate in this trial has been reproduced in other settings, with a response rate of 36.4% in a pooled analysis of four large trials for nivolumab monotherapy.[14] Similar to ipilimumab, it appears that many of these responses are durable, with five-year survival rates from the earliest phase I trial recently reported as 34%.[15]

Results from the phase III melanoma trial of pembrolizumab monotherapy largely mirrored those of nivolumab. Patients in the arm receiving pembrolizumab injections every two weeks had a 33.7% objective response rate, with 13.3% of patients experiencing grade 3 or 4 toxicity.[16] A recent meta-analysis showed a similar ORR of 33% in 655 patients with a median overall survival of 23 months.[17] While 14% patients experienced grade 3 or 4 adverse events, only 4% of patients stopped therapy because of toxicity.

More recently, investigators have focused on combining PD-1 and CTLA-4 blockade. The three-arm Checkpoint 067 trial compared the combination of ipilimumab and nivolumab against both nivolumab and ipilimumab monotherapies. Treatment response was 57.6% for combination therapy, compared to 43.7% for nivolumab monotherapy and 19.0% for ipilimumab monotherapy. Similarly, PFS was 11.5 months for the combination arm compared to 6.9 months with nivolumab and 2.9 months with ipilimumab. However, Grade 3-4 adverse events were observed in 54% of patients in the combination arm, compared to only 20% of those receiving ipilimumab alone.[18] A recent pooled analysis of 1250 patients also showed higher ORR, longer PFS, and higher toxicity with combination compared to nivolumab monotherapy in both mucosal and cutaneous melanoma.[19]

In an effort to reduce the immune toxicities with combined therapy, efforts are ongoing to study sequential treatment with nivolumab and ipilimumab. While few results have been published, it has been reported that response rate at 25 weeks with nivolumab followed by ipilimumab (41%) may be twice as high as in patients treated with the

reverse sequence (20%).[20] These initial data will be helpful in the design of pending studies comparing sequential and concomitant therapy.

PD-L1 as a predictive biomarker for anti-PD-1 immunotherapy

In a majority of clinical trials for nivolumab and pembrolizumab, immunohistochemical assays for PD-L1 have been performed on paraffin-embedded pre-treatment tumor samples in an effort to identify patients most likely to respond to these agents. In the phase III CheckMate 066 trial of nivolumab, the ORR was higher for patients with PD-L1 positive tumors (53% v. 33%).[13] However, both PD-L1 positive and negative groups receiving nivolumab had a significant survival benefit compared to the control arm. Similarly, in the KEYNOTE-001 trial of pembrolizumab, PD-L1 positivity was associated with better PFS and better OS.[21]

Despite these promising findings, the cumulative results of PD-L1 as a predictive biomarker have been mixed; many responses in PD-L1-negative tumors remain unexplained. Unlike in other cancer types (e.g., non-small cell lung cancer treated with pembrolizumab), there are no FDA-approved companion or complementary diagnostics based on PD-L1 for the treatment of melanoma. In a pooled analysis of four nivolumab trials including 440 melanoma patients, PD-L1 status did not affect objective response rates.[14] Importantly, PD-L1 has not been shown to be an effective predictive biomarker for combination checkpoint blockade. In the CheckMate 069 trial of nivolumab and ipilimumab, PD-L1 expression was not associated with significantly higher ORR. Similarly, PD-L1 expression was not associated with higher PD-L1 expression in the combination arm of the CheckMate 067 study. Given the improved efficacy and increased frequency of immune-related toxicities with combination ipilimumab and

nivolumab, biomarkers for identifying the patients likely to respond to to this regimen remain a major unmet clinical need.

There are multiple hypotheses that could explain the limited positive and negative predictive power of PD-L1 in this setting. Variability of semi-quantitative assays across trials is one of potential source of case mis-classification. In addition to using different sets of immunohistochemical reagents, trial sponsors empirically set different semi-quantitative cutoffs to identify PD-L1 positive and PD-L1 negative cutoffs. For instance, in the phase III trial of nivolumab, PD-L1 positivity was defined as at least 5% tumor cells showing PD-L1 cell surface staining as determine by a pathologist.[13] In contrast, the threshold for positivity was set as 1% in the phase III trial of pembrolizumab.[16]

It is also possible that antibody binding is affected by post-translational modification of PD-L1, leading to false-negative or false-positive assay results. PD-L1 has four potential N-linked extracellular glycosylation sites in its IgV-like and IgC-like domains.[22] Antigen glycosylation has been shown to affect the binding of antibodies in other settings,[23-25] and the epitopes of commercial antibodies are not publicly disclosed. Thus, it is possible that one or more of commercial antibodies target these glycosylated residues. As few data are available of the patterns of PD-L1 glycosylation in human tumors or their biological relevance, it may be important to assess the binding of several anti-PD-L1 antibodies to their antigen in both glycosylated and unglycosylated conditions.

A better-documented explanation for PD-L1's relatively poor performance as a predictive biomarker is its markedly heterogeneous staining pattern.[26] In multiple tumor types, PD-L1 is often focally expressed in close proximity to lymphocytic infiltrates near

the tumor-stromal interface.[27] In melanoma, PD-L1 expression correlates with higher CD8+ infiltrates across multiple anatomic sites.[28] These observations have been further developed into a model of adaptive immune evasion, in which secretion of interferon gamma (IFNγ) by infiltrating immune cells locally activates JAK/STAT signaling in tumor cells and induces focal expression of PD-L1.[29-32] In this context, it is possible that spatial or temporal sampling error could account for some of the yet-unexplained responses to anti-PD-1 therapy in PD-L1 negative tumors. PD-L1 can also be constitutively expressed downstream of tumor-intrinsic oncogenic pathways; it remains unclear if the manner of PD-L1 induction confers differential susceptibility to checkpoint ability for response to immunotherapy.

Interferon gamma signaling & IRF-1 as candidate predictive biomarkers

Given the heterogeneity of PD-L1 expression, identifying a tumor's capability to express PD-L1 under the appropriate inflammatory conditions might identify a broader range of cases able to respond to anti-PD-1 agents than assessment of PD-L1 alone. Specifically, we considered the expression of the PD-L1 transcription factor interferon regulatory factor-1 (IRF-1) as a possible marker for this capability. IRF-1 lies immediately upstream of PD-L1 in the IFNγ-driven JAK/STAT signaling cascade,[30] and has been shown to play a central role in regulating cancer cell's response to IFNγ.[33]

In brief, upon IFNγ binding, two transmembrane interferon gamma receptor heterodimers bind together into a four-peptide complex, which leads to the cross-phosphorylation of associated intracellular Janus kinases (Jak) proteins on their tyrosine residues as well as phosphorylation of intracellular receptor subunits. This phosphorylated complex recruits cytoplasmic STAT proteins, such as STAT1, which are

in turn phosphorylated and converted into antiparallel dimers that can traffic into the nucleus. There, STAT1 binds to promoters of primary interferon response genes, which include IRF-1.[29,34]

In addition to driving PD-L1 expression, IFNγ signaling has been previously implicated in antigen presentation and anti-tumor immune surveillance, including upregulation of both major histocompatibility complex I & II (MHC I & II).[35] Early studies demonstrated that tumors lacking either the IFNγ receptor (IFNGR1) or STAT1 grew faster in immunocompetent mouse hosts than tumors with intact JAK/STAT signaling.[36] Similarly, murine tumors with dominant negative interferon gamma receptors also had a growth advantage.[37] Interestingly, immunogenicity of IFNGR1 or STAT1 deficient tumors could be restored with overexpression of TAP1, a processing enzyme that loads MHC I tetramers with peptide antigens.[38] Taken together, these results could suggest that IFNγ-driven presentation of antigen is a critical step for immune surveillance of tumors.

Perhaps unsurprisingly, IFNγ signaling has been implicated as important for responses to immune checkpoint blockade. Tumeh et al. reported higher phosphorylated STAT1 levels higher in both pre-treatment and on-treatment tumor samples from melanoma patients responding to PD-1 blockade than those that progressed on therapy.[31] However, immunohistochemical assays for phosphorylated antibodies in paraffin embedded tissue have historically not been highly reproducible. Further evidence has come from genomic analyses, including the identification of IFNγ related mRNA signatures in pretreatment associated with response to anti-PD-1 therapy.[39] Also, acquired mutations in JAK1, JAK2, and the MHC I component beta-two-microglobulin were

found anecdotally in three patients who developed acquired resistance to pembrolizumab after initially responding to therapy.[40] The same group of investigators recently extended this finding to primary resistance to PD-1 blockade. In a small clinical series, 1 of 9 melanoma patients melanoma patients unresponsive to pembrolizumab carried homozygous mutations in JAK1, while 0 of 13 responders had homozygous mutations in any IFNγ signaling components or antigen presenting genes.[41]

Unlike other components of the JAK/STAT pathway, IRF-1 is generated *de novo* in response to IFNγ binding, making it uniquely amenable to immunohistochemical assays. IRF-1 is encoded by a single gene on 5q31, and was identified in 1988 as the first of nine members of the IRF family of transcription factors. All members of this class have a conserved binding domain that recognizes interferon-stimulated response element sequences in the genome. IRF-1's various roles were first characterized in immune cells. It is required for the development of neutrophils and macrophages, and can drive the development of a T_H1 phenotype in CD4+ T cells. Like NF-KB, IRF-1 has a role in innate immunity—it can stimulate secretion of pro-inflammatory cytokines downstream of pattern recognition receptors. Specifically, engagement of TLR9 causes IRF-1 to more efficiently migrate to the nucleus, where it exerts its transcriptional control.[42]

Roles for IRF-1 in cancer have also been identified. As a tumor suppressor gene, IRF-1 was shown to be necessary for DNA-damage associated growth arrest and apoptosis.[42] Loss of one IRF-1 allele has been correlated with gastric and esophageal cancers, suggesting that a second-hit mutation may promote oncogenesis.[43] In melanoma, IRF-1 can be induced in a subset of melanoma cell lines; those that were not inducible

had distinct mRNA profiles, with lower levels of mTOR and Wnt/beta catenin transcriptomic signatures.[44]

IRF-1 is also necessary for constitutive and induced PD-L1 expression in cancer.[30] While it is possible that IRF-1 expression correlates with that of PD-L1, detection of this transcription factor may represent a cell state that is capable of expression of PD-L1 when facilitated by local molecular microenvironment. For example, deubiquitination of PD-L1 by CSN5 has recently been shown to be an important post-translational regulatory process affecting PD-L1 protein levels.[45] PD-L1 is also regulated by other mechanisms, including signaling pathways mediated by PTEN,[46,47] mTOR,[48] and EGFR.[49]

Immune activation as a candidate predictive biomarker

As IFNγ signaling is initiated by the secretion of IFNγ by tumor-associated immune infiltrates, it is also worth considering whether these infiltrates themselves can be assayed to predict response to immunotherapy. Melanoma has long been known to be among the most immune-rich tumors—in the 1960s, the pathologist A.J. Cochran reported that 37% of a series of 165 melanomas had lymphoid aggregates at their periphery and that an additional 35% were associated with a mixture of lymphocytes and plasma cells.[50] It was later reported that higher levels of tumor-infiltrating lymphocytes (TILs) in primary cutaneous melanomas in the vertical growth phase were associated with more favorable prognoses.[51]

Preclinical studies of the PD-1/PD-L1 axis suggested that the CD8+ T cell population may have a role as a predictive biomarker for anti-PD-1 immunotherapy, as

CD8+ cells were required for PD-L1 expression, as well as the recruitment of inhibitory

T_{reg} cells, in a ectopic mouse model of melanoma.[52] However, the association between

CD8+ cells in pretreatment tissue samples and response has not been robust. While

Tumeh et al. demonstrated an association in melanoma between CD8+ cells at the tumor

margin with response to pembrolizumab,[31] Taube et al. reported no such association in a

mixed cohort of renal cell carcinoma, melanoma, and NSCLC treated with nivolumab.

Interestingly, the former study also reported an increase in immune activation with the

start of therapy, as measured by immune cell expression of Ki67, a marker of

proliferation, and cytolytic Granzyme B.

As an extension of this finding, it is possible that interrogating the pre-treatment

activation status of TILs—as measured by Ki67 and Granzyme B—in melanoma

specimens could potentially identify patients most likely to respond to anti-PD-1

checkpoint blockade. While a basal level of activation may be required for further

immune response with PD-1 blockade, alternatively, tumors with the greatest levels of

quiescent TILs may benefit most from targeting this inhibition.

Soluble PD-L1 as a candidate predictive biomarker

In addition to tissue-based biomarkers, liquid biomarkers from the peripheral

blood are gaining traction in the practice of oncology. Liquid biomarkers can be assayed

with routine blood draws, and can thus be collected at more frequent intervals than tissue

biopsies to track tumor evolution and gauge response to treatment. Clinically, this

approach has advanced most rapidly in the treatment of non-small cell lung cancer

(NSCLC)—in June 2016, the first blood-based assay for EGFR mutations was approved

by the Food and Drug Administration. Early studies have shown that blood-based assays for genetic alterations in NSCLC provide complementary information to tissue biopies,[53] and that they may be more sensitive for resistance mutations such as EGFR T790M given the heterogeneity of tumor subclones.[54]

Given the heterogeneous expression of PD-L1 protein, it is possible that a plasma-based assay for soluble PD-L1 (sPD-L1) protein may provide a more integrated measure of expression across the tumor and various metastases. In 2007, a soluble form of the closely related immune marker CD80 was identified; this isoform was generated through alternative splicing and retained its ability to bind to its receptor, CD28.[55] Soluble PD-L1 detected by enzyme-linked immunosorbent assay (ELISA) was reported in metastatic renal cell carcinoma in 2011. In a study of 172 patients, sPD-L1 was higher in patients with T3 and T4 stage tumors and higher nuclear grade. sPD-L1 retained the PD-1 binding domain and was able to promote apoptosis in T cells, and a univariate survival analysis showed that a doubling of sPD-L1 led to an increased risk of death, though this did not remain significant in a multivariate survival model.[56]

sPD-L1 was shown to vary with treatment response in a French study of 288 patients with diffuse large B cell lymphoma (DLBCL).[57] In pre-treatment samples, sPD-L1 was higher in patients with DLBCL than in healthy controls, and higher levels were associated with poorer prognosis in patients treated with CHOP chemotherapy regimen. After treatment, levels decreased in patients that experienced a complete remission. This suggests that in addition to serving a prognostic role, sPD-L1 may be used longitudinally to assess treatment response to anti-PD-1 therapy.

Less data has been published on sPD-L1 in tumor types treated commonly treated with anti-PD-1 immunotherapy, such as NSCLC and melanoma. A Chinese study of NSCLC showed that sPD-L1 was higher in patients compared to healthy controls, and that levels were higher in patients with adenocarcinomas compared those with squamous cell carcinomas.[58] It remains to be seen whether sPD-L1 could serve as a predictive biomarker for response to anti-PD-1 immunotherapy in either melanoma or NSCLC.

II. PURPOSE & SPECIFIC AIMS

Given the limited predictive value of current clinical assays for PD-L1 protein expression, this study will evaluate alternative biomarkers to predict response to anti-PD-1 immunotherapy. Specific aims are:

1. To **compare quantitative immunohistochemical assays for IRF-1 and PD-L1** as predictive biomarkers for both objective radiographic response and progression-free survival in a retrospective cohort of melanoma patients treated with anti-PD-1 immunotherapy

2. To **evaluate a multiplex panel of immune activation** (CD3, Ki67, & Granzyme B) as a predictive biomarker using the same melanoma cohort and outcome measures as in Aim 1.

3. To **evaluate a plasma-based assay for soluble PD-L1 protein** in the plasma of patients with NSCLC and healthy controls.

III. METHODS

IRF-1 and PD-L1 induction in cell lines

Melanoma cell lines were grown to 80% confluency, serum-starved for 24 hours and then treated with IFNγ or control media for 24 hours. Cells were then fixed directly on chamber slides, lysed for Western blotting, or fixed with formulate to generate paraffin-embedded (FFPE) pellets. Cells grown on chamber slides were washed twice in 1X phosphate-buffered saline (PBS) and then fixed in 4% paraformaldehyde (PFA) with 88 mM sucrose. For FFPE cell pellets, five ten-centimeter plates grown to confluency were first rinsed with PBS, and fixed in a solution 4% PFA at 4° Celsius overnight. Cells were then resuspended and rinsed three times in PBS before being washed twice in 80% ethanol (EtOH). Cell pellets were spun at 12,000 RPM and embedded in 2.2% melted agarose in PBS. Agarose-embedded pellets were incubated in 70% EtOH overnight and then sequentially dehydrated with one-hour incubations of 90% EtOH and 100% EtOH, two one-hour xylene washes, and submerged in molten paraffin for two hours before embedding. IRF-1 and PD-L1 induction in cell lines was performed by Lauren Moore. Cell pellets were generated by James Smithy.

Antibody Validation

Antibodies for IRF-1 (CST D5E4; #8478) and PD-L1 (Spring Bioscience SP142; #M4420) were validated[59] by immunoblotting and immunofluorescent staining. Upon treatment with IFNγ, melanoma cell lines upregulated IRF-1 and PD-L1 as detected by Western Blot (Figure 1A) and immunofluorescence (Figure 1B). Immunofluorescent

staining for IRF-1 was limited to the nucleus, while PD-L1 expression was detected in the membrane and cytoplasm. Progressively increasing expression of each marker seen with increased IFNγ stimulation was used to confirm specificity. Immunofluorescent staining and image analysis was performed by James Smithy.

Western blot

Cells were lysed in ice-cold M-PER mammalian Protein Extraction Reagent (Thermo Scientific) supplemented with protease inhibitors. To determine protein concentration a Bradford assay was conducted using the Bio-Rad protein assay reagent (Bio-Rad,). Proteins (30 µg) were subjected to sodium dodecyl sulfate-polyacrylamide gel electrophoresis (SDS-PAGE) and transferred to a nitrocellulose membrane (GE Healthcare). The resulting blots were blocked for 1 hour at room temperature (RT) in 5% skimmed dry milk diluted in 1X Tris-buffered saline supplemented with Tween-20 (TBST). Blots were incubated at 4ºC overnight in primary antibodies specific for PDL-1 (Spring Bioscience Clone SP142; diluted 1:500) or IRF-1 (Cell Signaling Technology Clone D5E4; diluted 1:1000). Following incubation, blots were washed with 5% milk/TBST before incubation with a horseradish peroxidase, labeled goat anti-rabbit IgG (Santa Cruz Biotechnology Inc.; diluted 1:5000) at RT for 1 hour. Blots were washed with 5% milk/TBST and bands were visualized using electrochemiluminescence detection reagents (Thermo Scientific). Western blots were performed by James Smithy and Lauren Moore.
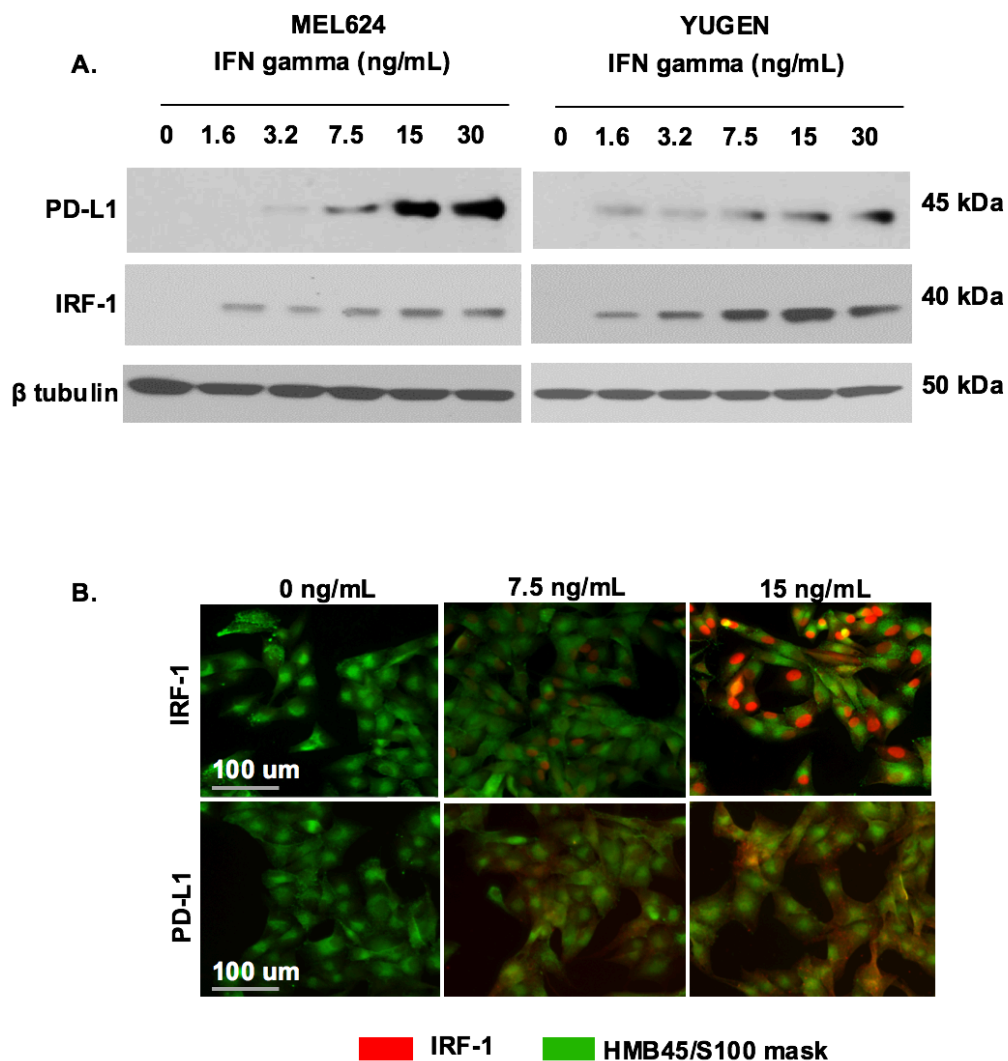
Figure 1. IRF-1 assay validation in cell lines and melanoma cases. A. Induction of IRF-1 and PD-L1 with increasing concentrations of interferon gamma in YUGEN and Mel624 melanoma cell lines by Western blot. B. Induction of IRF-1 and PD-L1 in YUGEN melanoma cells by immunofluorescence. Green (Cy3 channel) = HMB45/S100 tumor mask. Red (Cy5 channel) = target.

Case identification for melanoma cohort

Medical records and tissue samples were identified for melanoma patients with non-ocular primary tumors treated with pembrolizumab or nivolumab within the Yale-New Haven Health system before April 1, 2016 under a protocol approved by Yale Human Investigations Committee. 51 cases with available pre-treatment tissue specimens were identified and selected by a board-certified pathologist. Of these, 47 had appropriate imaging available (e.g., CT, PET, and/or MRI) to determine response and PFS by objective criteria. Of the 47 cases, 21 (45%) demonstrated a partial or complete response, including one case of pseudo-progression. Objective radiographic response (ORR) and PFS were determined by review of available CT or MRI scans using modified RECIST v1.1 criteria.[60] To account for the possibility of pseudo-progression,[61] progression at first follow up scan needed to be confirmed with further progression at a second follow up scan to be classified as PD. Twenty-eight cases (60%) were treated with single-agent pembrolizumab or nivolumab and 19 cases (40%) were treated with combination ipilimumab and nivolumab. Additional cohort characteristics are described in Table 1. The response rates in the monotherapy and dual therapy arms were 46% and 42%, and the median PFS were 5.9 and 6.1 months, respectively. Case identification, abstraction of clinical data, and assessment of response was performed by James Smithy. Identification of appropriate samples for staining was performed by James Smithy and Vasiliki Pelekanou.

		All patients	IRF-1 High	IRF-1 Low
N		47	31	16
Median age at diagnosis		62	63	60
Sex	Male	24	14	10
	Female	23	17	6
Race	White	44	30	14
	Black	2	0	2
	Hispanic	1	1	0
Treatment	Pembrolizumab	18	12	6
	Nivolumab	10	4	6
	Ipilimumab + nivolumab	19	15	4
Prior checkpoint blockade	Yes	16	11	5
	No	31	20	11
Mutation status	BRAF	16	11	5
	NRAS	6	5	1
	CKIT	2	2	0
	None detected	23	13	10
Stage at diagnosis	I	5	3	2
	II	8	5	3
	III	17	11	6
	IV	11	8	3
	Unknown	6	4	2

Table 1. Clinical and pathologic characteristics for 47 metastatic melanoma cases with available pre-treatment tissue.

Quantitative immunofluorescence for single markers: IRF-1 & PD-L1

FFPE whole-tissue sections, tissue microarrays (TMAs) and cell pellets were processed and stained as previously described[62]. Briefly, sections were baked for 30 minutes at 60° C and underwent two 20-minute washes in xylenes. Slides were rehydrated in two 1-minute washes in 100% EtOH followed by one wash in 70% EtOH and finally rinsed in streaming tap water for 5 minutes. Antigen retrieval was performed in sodium citrate buffer, pH 6, for 20 minutes at 97°C in a PT module (LabVision). Endogenous peroxidases were blocked by 30-minute incubation in 2.5% hydrogen peroxide in methanol. Subsequent steps were carried out on the LabVision 720 Autostainer (Thermo-Scientific). Nonspecific antigens were blocked by a 30-minute incubation in 0.3% bovine serum albumin (BSA) in TBST. Slides were then incubated with the target primary antibody, as well as a cocktail of two mouse monoclonal antibodies against S100 (Clone 15E2E2, BioGenex) and HMB45 (Clone HMB45, Biogenex) each diluted at 1:100 to define the tumor compartment. IRF-1 was detected with rabbit monoclonal antibody clone D5E4 (Cell Signaling Technologies) at 0.6 ug/mL and PD-L1 was detected with rabbit monoclonal antibody SP-142 (Spring Biosciences) at 0.08 ug/mL.

Primary antibodies were followed by incubation with Alexa 546–conjugated goat anti-mouse secondary antibody (Life Technologies) diluted 1:100 in rabbit EnVision reagent (Dako) for 1 hour. Signal was amplified with Cy5-Tyramide (Perkin Elmer) for 10 minutes, and then nuclei were stained with DAPI in BSA-tween for 10 minutes. Slides were mounted with ProlongGold (Life Technologies). Two TBS-T and one TBS wash wash performed between each step after the primary antibody.

For cells fixed on chamber slides, samples were washed twice in PBS after fixation and permeabilized with 0.25% Triton X-100 in PBS for 10 minutes. Cells were washed twice in PBS and blocked with 1% BSA in PBS for 1 hour at room temperature. Block was decanted off slides and the primary antibody cocktail as described above was applied. Subsequent steps were identical to the staining of FFPE tissue, except the DAPI stain was substituted for mounting Prolong Gold with DAPI (Life Technologies). One PBS-T and one PBS wash were performed between each step after the primary antibody.

Immunofluorescence was quantified using automated quantitative analysis (AQUA) on all fields of view containing tumor on each slide. Briefly, fluorescent images of DAPI, Cy3 (Alexa 546-S100/HMB45), and Cy5 (PD-L1 or IRF-1) for each field of view (FOV)were collected. Image analysis was carried out using the AQUAnalysis software (Genoptix), which generated an AQUA score for each compartment by dividing the sum of target pixel intensities by the area of the compartment in which the target is measured[63]. PD-L1 was measured in the S100/HMB45-positive tumor compartment and IRF-1 was measured within the DAPI-positive nuclear compartment within the tumor compartment. A total AQUA score was determined for each case by averaging scores from each 20X field of view. Immunofluorescent staining, image capture, and image analysis were performed by James Smithy

Quantitative immunofluorescence for multiplex immune activation panel

FFPE cases were stained for the immune activation panel as described above through blocking in BSA/TBST, using a modified multiplex protocol on the LabVision 720 Autostainer (Thermo-Scientific) as previously described.[64] Primary antibodies

against CD3, granzyme B, and Ki67 antibodies were coincubated for one hour at room temperature. CD3 was detected with rabbit monoclonal antibody SP7 at 1:100 (Concentration unavailable, Novus Biologicals), Granzyme B was detected with mouse monoclonal antibody 4E6 (Abcam) at 500 ng/mL, and Ki67 was detected using mouse monoclonal MIB-1 (Dako) at (460 ng/mL). Slides were incubated sequentially with three horseradish peroxidase (HRP)–conjugated secondary antibodies for 1 hour at room temperature before tyramide-based HRP activation for 10 minutes, followed by 1 mmol/L benzoic hydrazide with 0.15% hydrogen peroxide to quench HRP activation. The secondary antibodies added sequentially were anti-rabbit Envision reagent (Dako), anti-mouse IgG1 (Abcam; 1:100) to detect the MIB-1, and anti-mouse IgG2a (Abcam; 1:200) to detect 4E6 primary. After each secondary step, HRP activators were biotinylated tyramide (PerkinElmer; 1:50), TSATMPlus Fluorescein tyramide (PerkinElmer; 1:100), and Cy-5 tyramide (PerkinElmer; 1:50), respectively. Subsequently, slides were incubated in Alexa 750– conjugated streptavidin for 1 hour (1:100; Invitrogen). Two mouse monoclonal antibodies against S100 (Clone 15E2E2, BioGenex) and HMB45 (Clone HMB45, Biogenex) and goat anti-mouse Alexa488 identified melanoma tumor compartment. DAPI identified nuclei. A schematic of this staining protocol is included in Figure 2.

Quantitative analysis of all fields of view containing S100/HMB45-positive tumor was performed using inForm Advanced Image Analysis Software version 2.x (Perkin Elmer). A spectral library was prepared using single stains of the following dye or fluorochromes: DAPI, FITC, Cy3, Cy5, and Cy7. Each dye or fluorochrome was separated into a discrete channel. Vectra III .im3 image files were loaded into the

software. Fluorochromes and dyes in the Vectra III images were unmixed using the spectral library. The tissues in the images were segmented into tumor and stroma areas with the use of the automated tissue segmenter embedded in the software. In each of the areas, individual cells were segmented into nuclei, cytoplasm, and membrane using stains in the nucleus and membrane as internal and external cell borders. This allows for isolation of individual cells and quantitation of cells by staining patterns. Thresholds for positivity was set for each stain based on optical density--cell-based scores for each marker were thresholded as follows to binarize cell populations into positive and negative subgroups: CD3 (Cy7): 1.5; Granzyme B (Cy5): 4; Ki67 (Cy3): 12.

Immunofluorescent staining and image capture were performed by James Smithy. Image analysis on Inform was performed by Kim Blenman, and statistical analysis was performed by James Smithy.

Chromogenic staining for IRF-1 & PD-L1

FFPE cases were stained for IRF-1 as described above through the secondary antibody incubation. Then, slides were incubated with 3,3'-diaminobenzidine peroxidase substrate (Vector Laboratories) for 8 minutes and counterstained with Tacha's Auto Hematoxylin (Biocare Medical). Slides were then dehydrated in washes of 70% EtOH, 100% EtOH, and xylenes before mounting. Single-plex chromogenic staining for PD-L1 on a serial section was performed using the FDA-approved 22C3 assay on the DAKO Link 48 automated staining platform. Staining for IRF-1 was performed by James Smithy and staining for PD-L1 was performed by Veronique Neumeister and John McGuire.
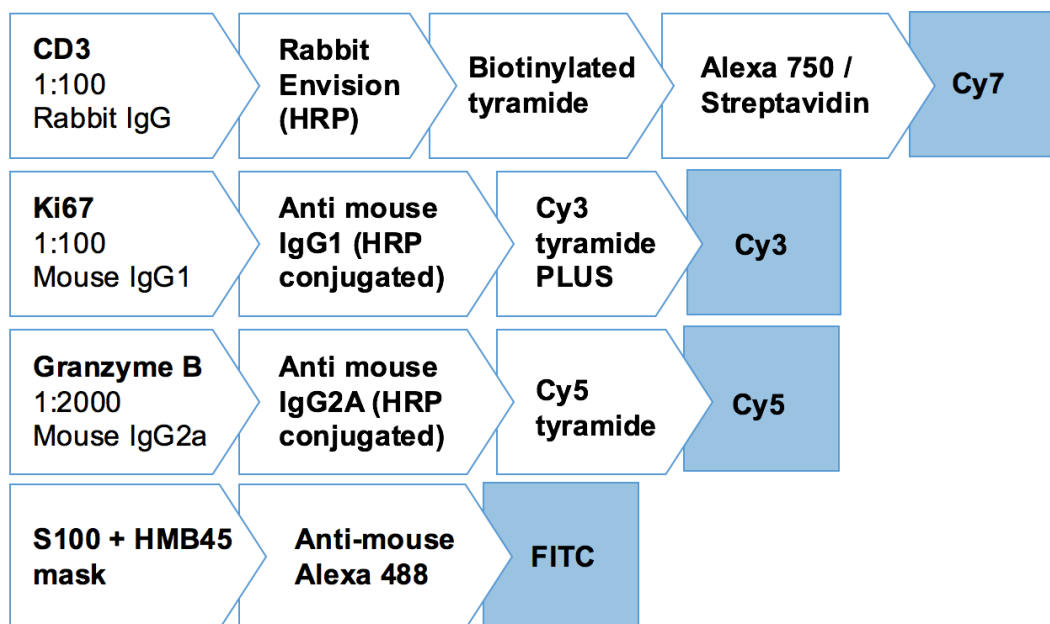
Figure 2. Schematic of immune activation panel staining protocol. Blue squares represent fluorescent channels in which each marker was detected.

PD-L1 deglycosylation

Lysates were prepared as described above for the melanoma cell lines mel624 (mel624 WT), mel624 transfected with overexpressed PD-L1 (Mel624 B7H1), and NSCLC cell lines H441, H820, and A549 treated with IFNγ (A549 + IFNγ). Lysates were diluted in PBS to generate 9 µg protein samples in 9 µL buffer. To each sample, 1 uL PNGase F denaturing buffer (New England Biolabs) was added and then samples were heated to 100°C for five minutes. Then, 1.25 µL 10% NP40 (New England Biolabs) and 1.25 uL 500 mM sodium phosphate pH 7.5 (New England Biolabs) were added before samples were sealed and incubated at 37°C for 3.5 hours.

Samples were then denatured for five minutes at 100°C with 10X LDS loading buffer (Thermo Fisher Scientific) and 10X reducing buffer (Thermo Fisher Scientific) before being loaded to SDS-PAGE gel. Western blots were performed as described above with the following three antibodies: E1L3N (Cell Signaling Technologies), E1J2J (Cell Signaling Technologies), and SP142 (Spring Biosciences). Deglycosylation and Western blots were performed by James Smithy.

Case identification for soluble PD-L1

Plasma samples from fifteen patients with non-small cell lung cancer treated with anti-PD-1 immunotherapy were obtained from the repository of Dr. Abhijit Patel in the Section of Therapeutic Radiology. Two patients had samples collected at two time points, for a total of 17 samples. Of these, nine samples were pre-treatment, five were on treatment, and three were post-treatment. The study cohort had a median age of 59 (range: 45-81) and was 40% male.

Plasma samples from 10 age- and sex-matched cancer-free controls undergoing unselected surgeries at Yale New Haven Hospital were collected from the Program for Applied Translational Research (PATR) biorepository within the Yale Section of Nephrology. The median age of control patients was 60 (range: 29-63) and 40% were male. To determine whether sPD-L1 is nonspecifically upregulated in inflammatory states, samples were analyzed at two time points for each control patient: pre-operatively as well as two-days postoperatively.

A second cohort of 47 plasma samples from NSCLC patients with known PD-L1 tumor status was obtained from the Thoracic Oncology tumor bank. Primary tumors from these patients had previously been assessed for PD-L1 staining by AQUA quantitative immunofluorescence.[26] Clinical and pathologic characteristics of this cohort are described in Table 2.

ELISA for soluble PD-L1

Human plasma samples were evaluated for soluble PD-L1 using Human B7-H1 DuoSet ELISA Kit (R&D Systems). Unless otherwise specified, reagents were included in the kit or in DuoSet ELISA Ancillary Reagent Kit 2 (R&D Systems). First, 96-well plates were incubated with 100 uL Capture Antibody at working concentration of 4 ng/mL in PBS overnight at room temperature. Wells were then washed three times with Wash Buffer, completely aspirating any liquid after each wash. Plates were blocked by adding 300 uL 1% BSA in PBS to each well for 1 hour at room temperature. At this point, and after each step before the addition of Substrate Solution, plates were washed three times as described above. Wells were incubated with 100 uL sample or standard in

triplicate and covered with an adhesive strip for two hours at room temperature. For antigen detection, plates were incubated for two hours with 100uL biotinylated detection antibody diluted in reagent diluent with 2% normal goat serum (Life Technologies). Streptavidin-HRP diluted 1:200 in 1% BSA/PBS was added to each well and incubated in the dark for 20 minutes. 100 uL Substrate Solution was added to each well and plates were incubated in the dark for 20 minutes. 50 uL Stop Solution was then added to each well, and plates were gently tapped to mix reagents.

Plates were then immediately read at 570 nm and 450 nm using a ELx800 plate reader (Biotek). Readings at 570 nm were subtracted from readings at 450 nm to correct for optical imperfections in the plate.

Estimation of sPD-L1 concentration in patient sample was made by comparing sample readings to those from standard curves. Standard curves were generated with a serial dilution of recombinant PD-L1 diluted in the plasma of the investigator, who has no known medical comorbidities. ELISAs for sPD-L1 were performed by James Smithy.

Statistics

AQUA scores between responders (PR/CR) and non-responders (SD/PD) were compared using an unpaired t test; PFS and OS between groups were compared using the log-rank test. A Cox proportional hazards model was constructed with age, sex, race, mutational status, prior checkpoint blockade, and IRF-1 status. All univariate statistical analyses was performed using GraphPad Prism 7 (GraphPad Software), and multivariate analysis was performed with JMP 11 (SAS Institute). All statistical analyses were performed by James Smithy

N		47
Median Age (Range)		69 (39-83)
Sex	Male	18
	Female	29
Smoking status	Current	4
	Former	37
	Never	4
	Unknown	2
Pack Years	0	4
	1-10	3
	11-25	12
	26-50	15
	51+	7
	Unknown	6
T stage	1	12
	2	17
	3	5
	4	2
Node status	Positive	9
	Negative	38
Histology	Adenocarcinoma	34
	Squamous	10
	Large cell	2
	Other neuroendocrine	1

Table 2. Clinical and pathologic characteristics for 47 NSCLC cases with matched plasma and tumor samples.

IV. RESULTS

IRF-1 as a prognostic biomarker in metastatic melanoma

To identify IRF-1 expression patterns in melanoma tissue, two TMAs of unselected metastatic melanoma cases (YTMA 98 and YTMA 59) were stained for IRF-1 (Figure 3A). Of 115 tumor cases on YTMA 59, 28 exhibited identifiable nuclear staining; average AQUA scores for these positive cases ranged from 204 to 723 (Figure 3B). We then sought to assess whether IRF-1 is a prognostic factor in melanoma irrespective of treatment. Cases from TMA 59 were stratified into IRF-1-high and IRF-1-low cohorts using an AQUA cutpoint of 204 based on the threshold for visual positivity. In this cohort, IRF-1 did not predict overall survival (OS) (Figure 3C) or disease-specific survival (Figure 3D).

IRF-1 as a predictive biomarker for anti-PD-1 immunotherapy

To assess IRF-1 as a predictive marker for response to PD-1 blockade, serial whole-tissue sections from 47 melanoma patients treated with anti-PD-1 immunotherapy were then stained for IRF-1 and PD-L1 in three batches. Batch-to-batch assay reproducibility was assessed by correlating scores from an index tissue microarray run with each batch (Figure 4). The median number of 20X fields of view per case was 64 for IRF-1 (range: 4 - 667), and 64 for PD-L1 (range: 7 - 764). There were trends toward higher expression of both markers in metastases compared to primary tumors, and in patients treated with prior checkpoint blockade compared to patients without prior treatment, though these differences did not reach statistical significance (Figure 5). There

was also a trend toward higher IRF-1 and higher PD-L1 in BRAF-mutant tumors compared to tumors without a known driver mutation (Figure 6, p = 0.06 for both markers). PD-L1 was higher in NRAS mutated tumors than in tumors without a known driver mutation (Figure 6B, p = 0.0003).

When classified by best ORR, AQUA scores for nuclear IRF-1 expression were higher in patients with PR/CR than in patients with SD/PD (p = 0.044, Figure 7A). There was a trend toward higher PD-L1 expression in patients with PR/CR (p = 0.085, Figure 7B), though this did not reach statistical significance. We then compared PFS from the start of therapy by IRF-1 expression level. PFS was related to ORR, but there was wide variability in PFS in the PR/CR and SD groups (Figure 8). Treated cases were then stratified into IRF-1-high and IRF-1-low cohorts using the lowest tertile as the IRF-1-low cohort (AQUA cutpoint = 194). PFS from the start of therapy was significantly higher in the IRF-1-high group than the IRF-1-low group (p = 0.017, Figure 7C). There was a trend toward higher OS in the IRF-1 high group, though this did not reach statistical significance (p = 0.060). To determine if there was biologic significance to this cutpoint, we determined the limit of detection for IRF-1 by staining five serum-starved melanoma cell lines for IRF-1 and identifying the lowest AQUA score a FOV with positive nuclear staining. Of five cell lines, only YUSOC had positive IRF-1 staining in the absence of IFN γ, and the lowest FOV AQUA score was for YUSOC was 171 (Figure 9). When the cohort was stratified by this cutpoint, PFS was still higher in the IRF-1-high than the IRF-1-low group (p = 0.0386, data not shown). Similarly, cases were stratified into PD-L1-high and PD-L1-low cohorts using a visual cutoff of 120. There was no difference in PFS (p = 0.83, Figure 7D) or OS (p = 0.98) between these two cohorts.

PD-L1 expression correlated with IRF-1 expression with a Pearson's correlation coefficient of 0.52 (Figure 10A, p = 0.0002). However, within the PD-L1-low cohort, four cases were classified as IRF-1-high. An example of one of these cases with high IRF-1 and low PD-L1 is shown in 10B and C. Despite this small sample size, there was a trend toward better PFS in those patients compared to those classified as IRF-1-low, PD-L1-low (p = 0.083).

When patients were grouped by therapy (PD-1 inhibitors alone versus the combination with CTLA-4 inhibitors), IRF-1 predicted longer PFS in the combination ipilimumab/nivolumab group (Figure 11A, p = 0.0051), but this difference did not reach statistical significance in patients treated with single-agent nivolumab or pembrolizumab (Figure 11B, p = 0.22).

In a Cox proportional hazards model for PFS, IRF-1-low status conferred a hazard ratio of 7.13 (95% Confidence Interval: 1.98 – 29.55, p = 0.0023) when accounting for age, race, sex, mutational status, and prior checkpoint blockade. When this model was modified to include average tumor IRF-1 expression as a continuous variable, IRF-1 remained an independent predictor of longer PFS (p = 0.0036).

To determine if variable PD-L1 glycosylation partially accounted for case misclassification, three commercial antibodies were evaluated for their ability to bind glycosylated and deglycosylated forms of PD-L1 in an *in vitro* model. For each of the untreated cell lines with positive PD-L1 expression, PD-L1 was detected by Western Blot as a broad band centered at 50 kilodaltons using three antibodies (Figure 12). In cell lines treated with PNGase F, this band was resolved to a single narrow band at approximately 30 kD. Results across the three antibodies were identical, except PD-L1 was only

detected in its deglycosylated form by E1L3N A549 lung cancer cells treated with IFNγ.

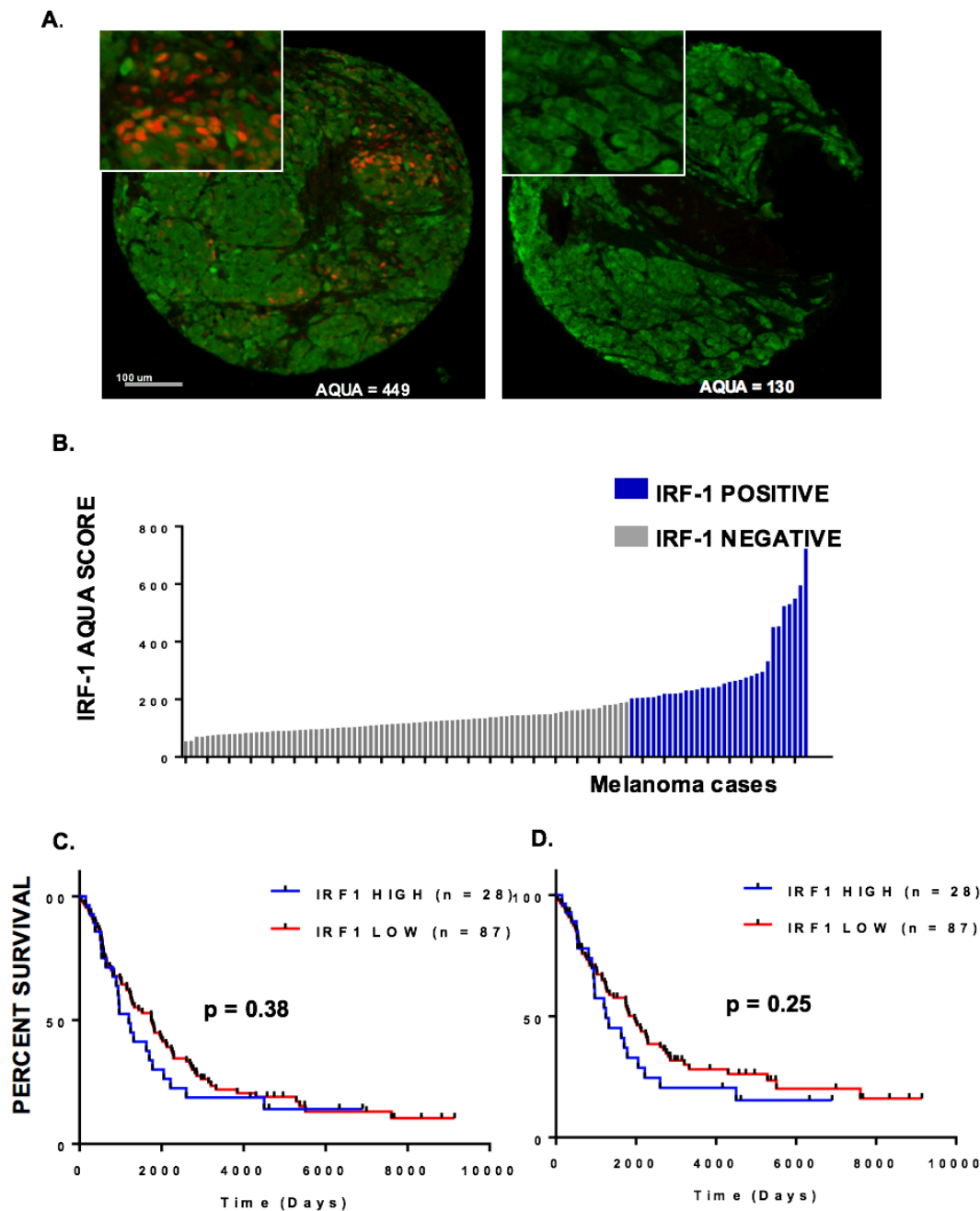No bands were observed with the negative control mel624 WT.

Figure 3. Characterization of IRF-1 in human melanoma samples. A) Representative IRF-1-positive and IRF-1-negative melanoma cases from Yale tissue microarray (YTMA) 98. Green (Cy3 channel) = HMB45/S100 tumor mask. Red (Cy5 channel) = target. 98 B) Average AQUA scores for nuclear IRF-1 for 115 melanoma cases on YTMA 115. Blue bars = visible nuclear staining. Gray bars = no nuclear staining. C) Overall survival in 115 melanoma cases unselected for treatment on YTMA 59 using visual cutpoint D) Disease-specific survival for cases on YTMA 59 using visual cutpoint
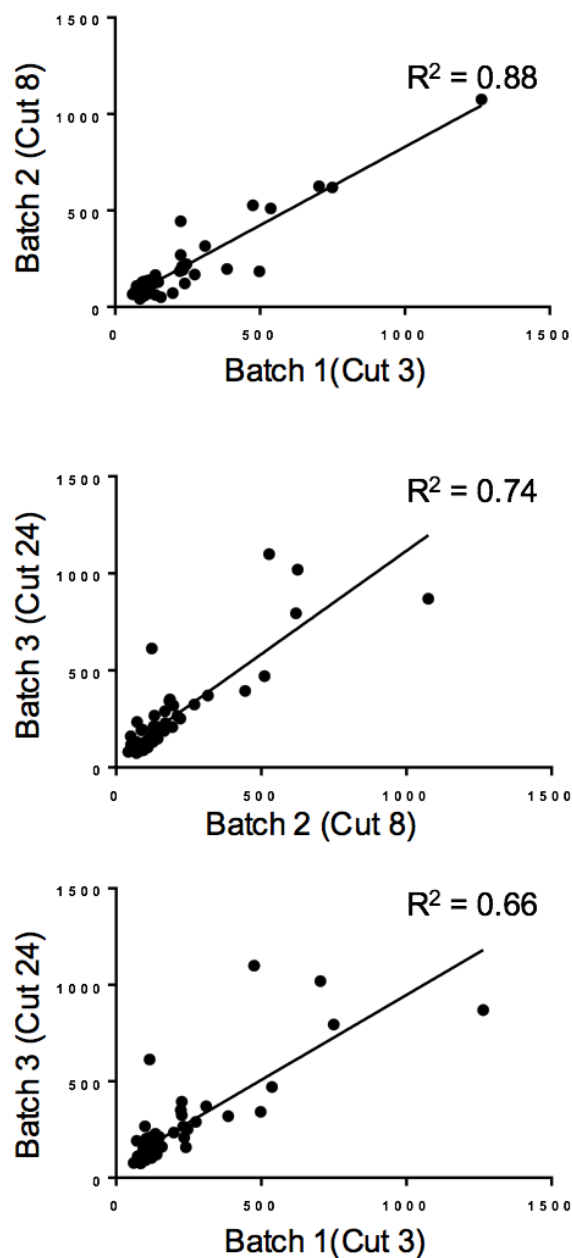
Figure 4. Batch-to-batch correlation of AQUA scores for index array (Yale TMA 343) run alongside whole-tissue sections as a control. Cut numbers reflect order of sections taken from block A) Batch 1 v. Batch 2. B) Batch 2 v. Batch 3 C) Batch 1 v Batch 3
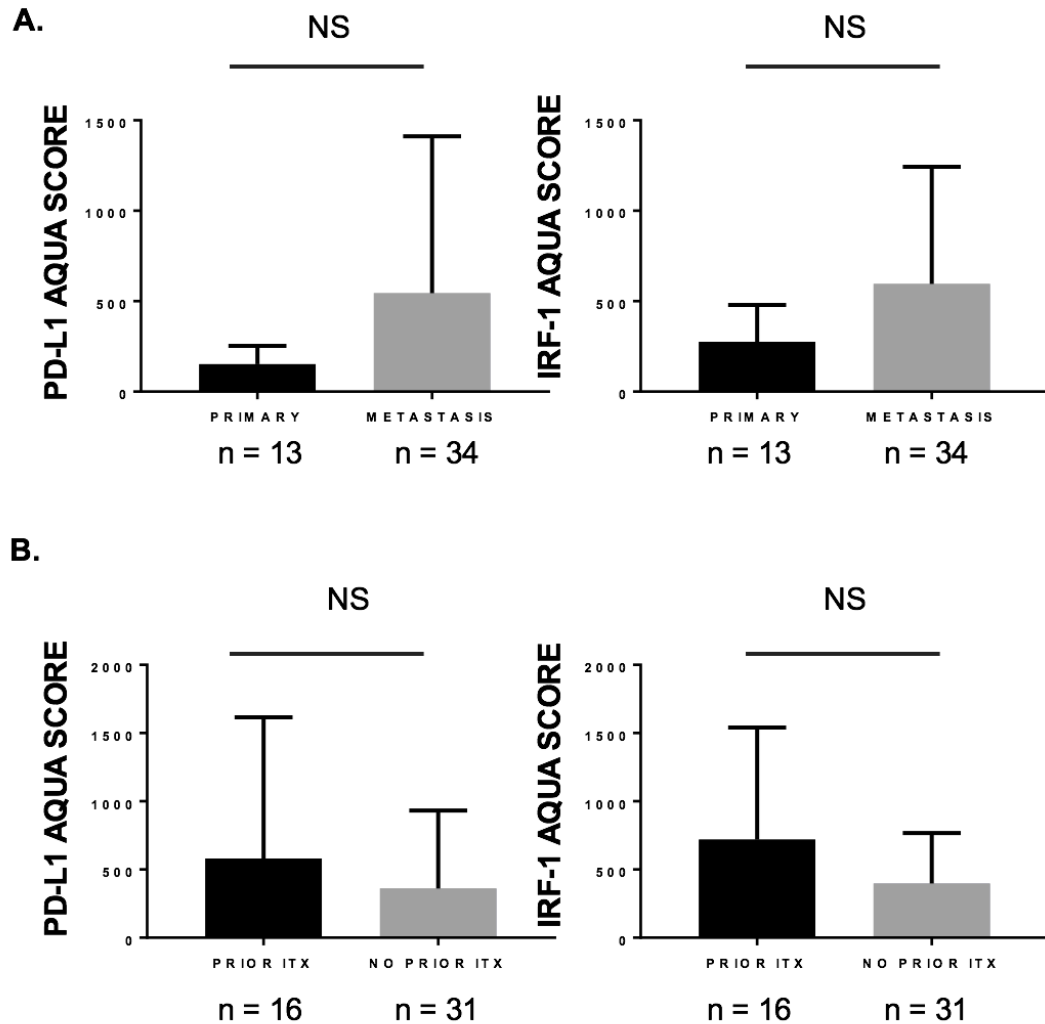
Figure 5. A) PD-L1 and IRF-1 expression in primary tumors and metastases (Mean +/- SD). B) PD-L1 and IRF-1 expression in patients treated with prior checkpoint blockade and in patients treated with first-line checkpoint blockade (Mean +/- SD).
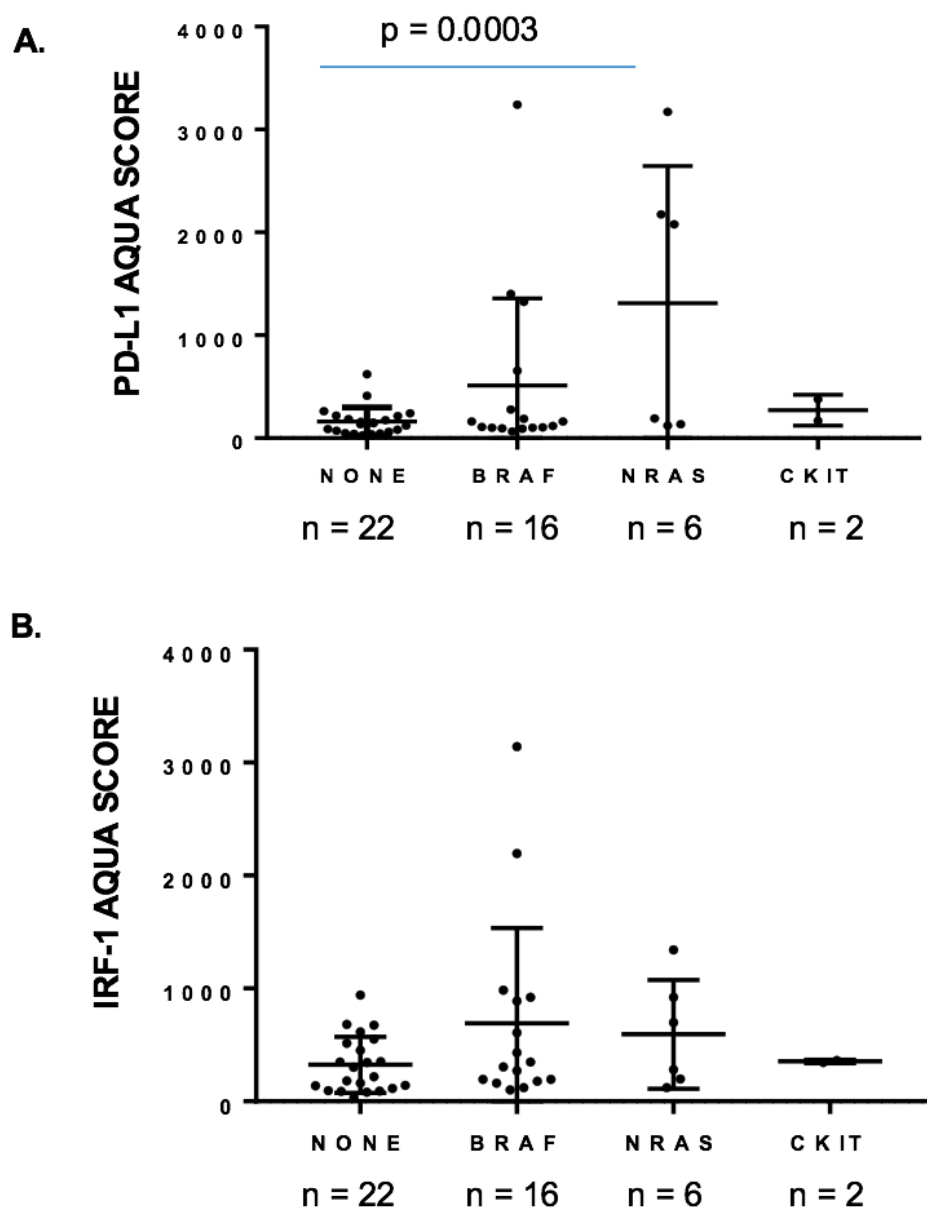
Figure 6. A) PD-L1 and B) Nuclear IRF-1 AQUA scores by melanoma mutational status. "None" refers to no known driver mutation identified by clinical molecular profiling. One tumor without recorded molecular profiling was excluded from this analysis
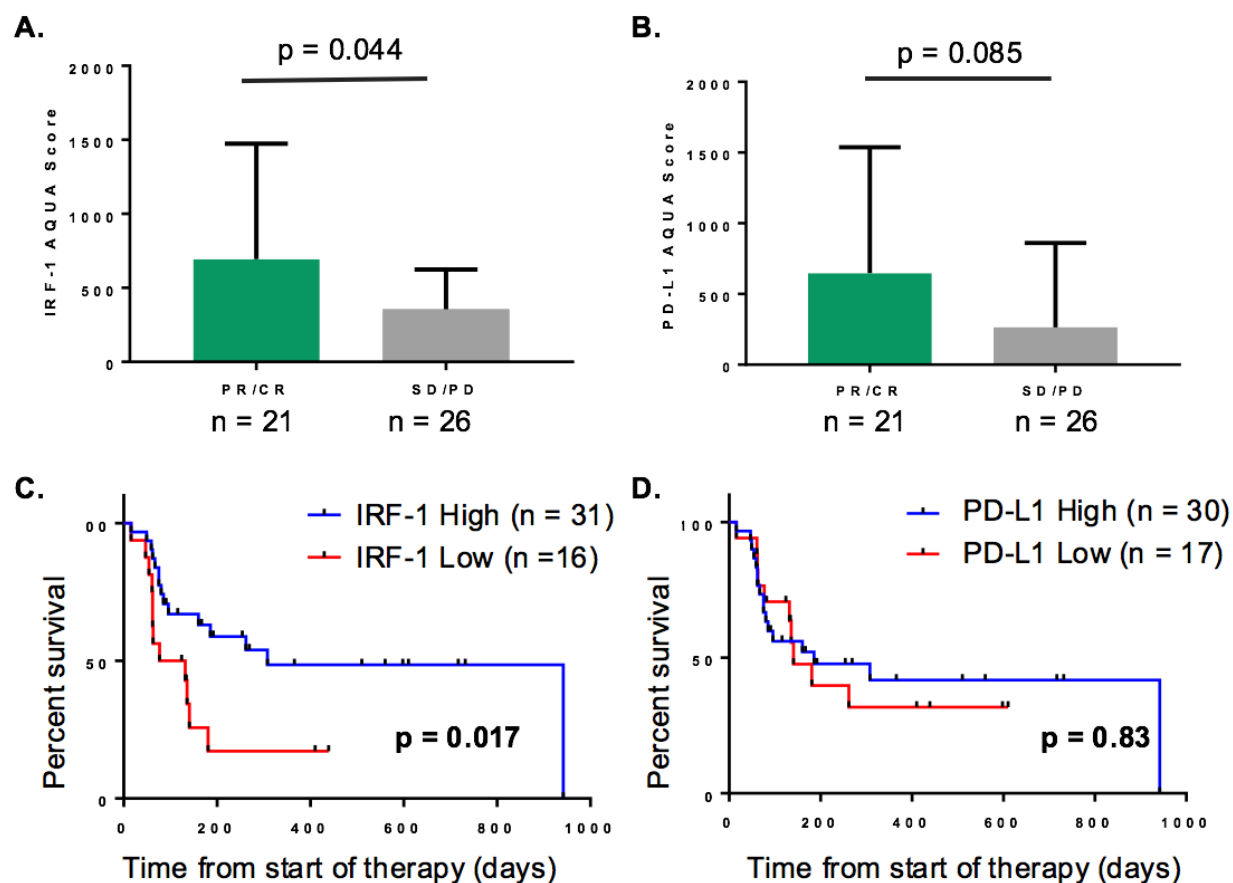
Figure 7. IRF-1 as a predictive marker for anti-PD-1 therapy. A) IRF-1 expression by best objective tumor response (Mean +/- Std Dev) B) PD-L1 by ORR (Mean +/- SD). C) Progression-free survival from the start of therapy stratified by IRF-1 expression level) D) Progression-free survival from the start of therapy stratified by PD-L1 expression level
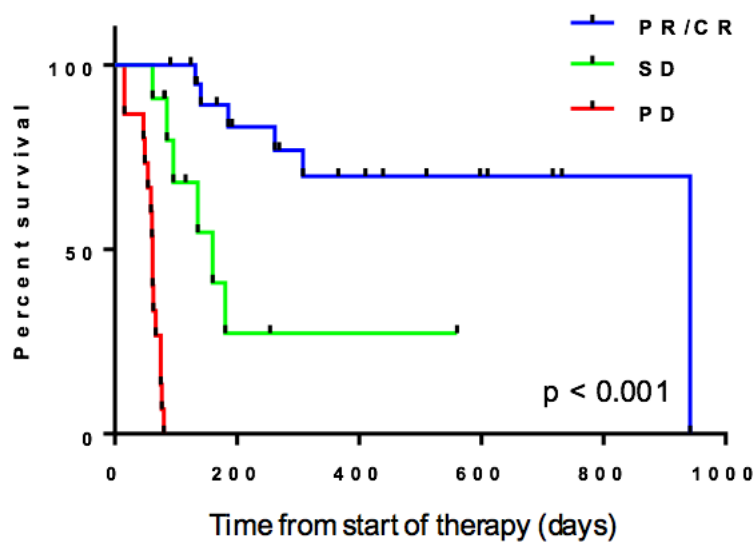
Figure 8. Progression-free survival from start of therapy by best objective radiographic response.
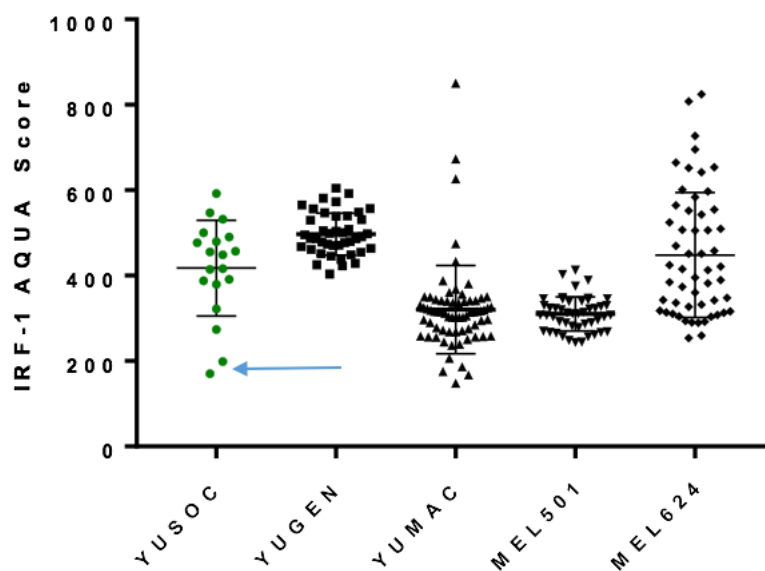

Figure 9. Nuclear AQUA scores for in FFPE pellets of five serum-starved melanoma cell lines. Green = nuclear IRF-1 staining. Black = nonspecific background. Arrow = limit of detection (AQUA = 170).
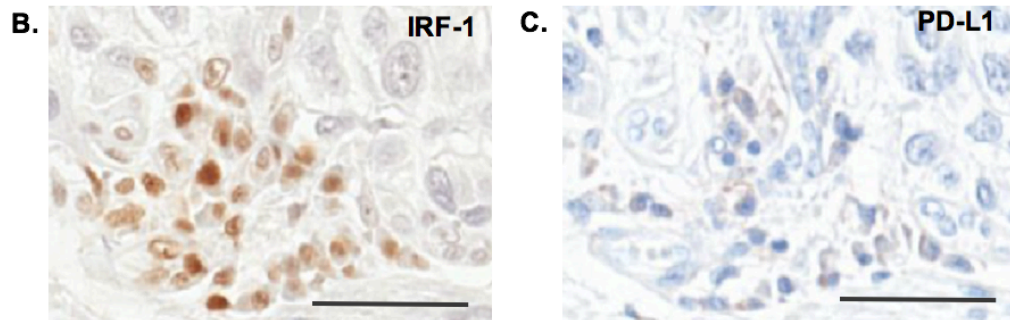
A.

B. IRF-1

C. PD-L1
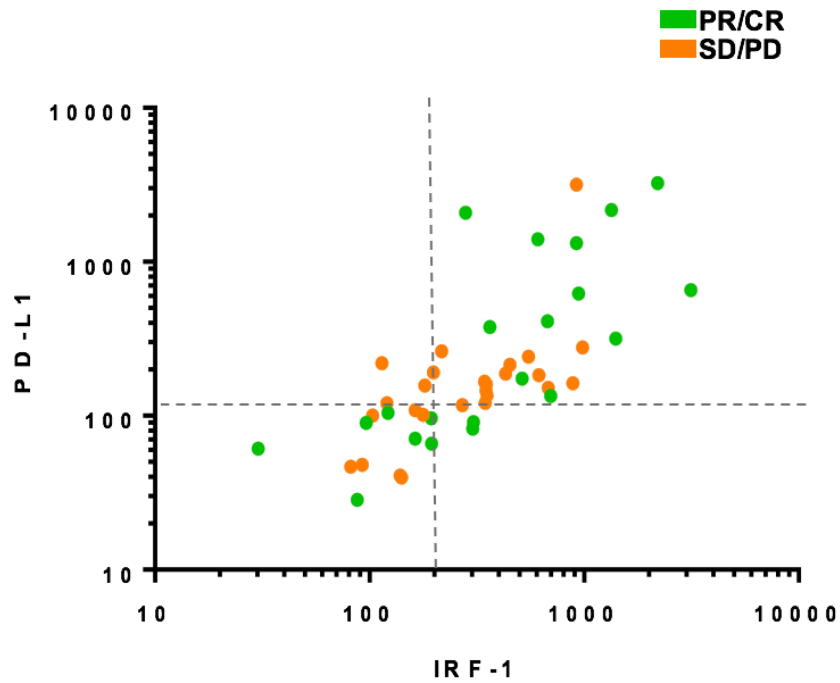
Figure 10. Relationship between PD-L1 and IRF-1 expression. A) Correlation of IRF-1 with PD-L1 (p = 0.002). Dashed lines represent cutoffs between high and low expression cohorts for PD-L1 and IRF-1 B), C) Serial whole-tissue sections showing chromogenic IRF-1 and PD-L1 IHC staining in a patient in the IRF-1-high, PD-L1-low cohort. Scale bar = 50 uM

Figure 11. A) PFS in by IRF status in patients treated with combination ipilimumab/nivolumab. B) PFS by IRF-1 status in patients treated with single-agent pembrolizumab or nivolumab,

Figure 12. Detection of degylcosylated PD-L1 in five cell lines by Western blot with three anti-PD-L1 antibodies. A) E1L3N at 1:1000; B) E1J2J at 1:5000; C) SP142 at 1:500
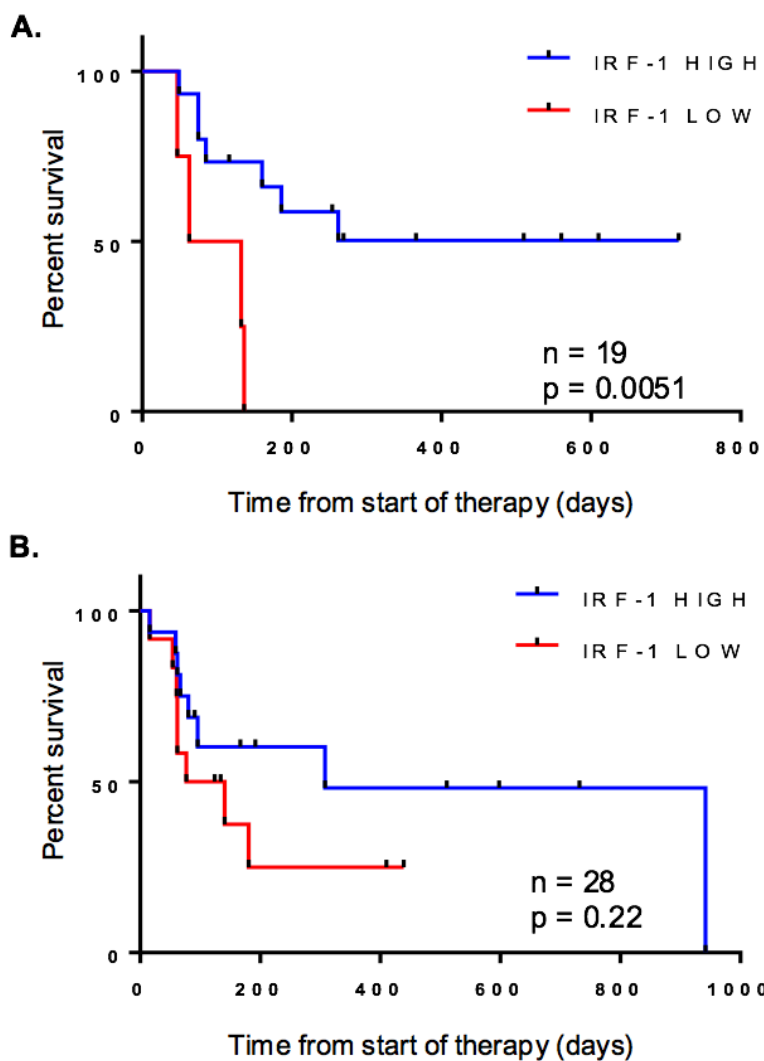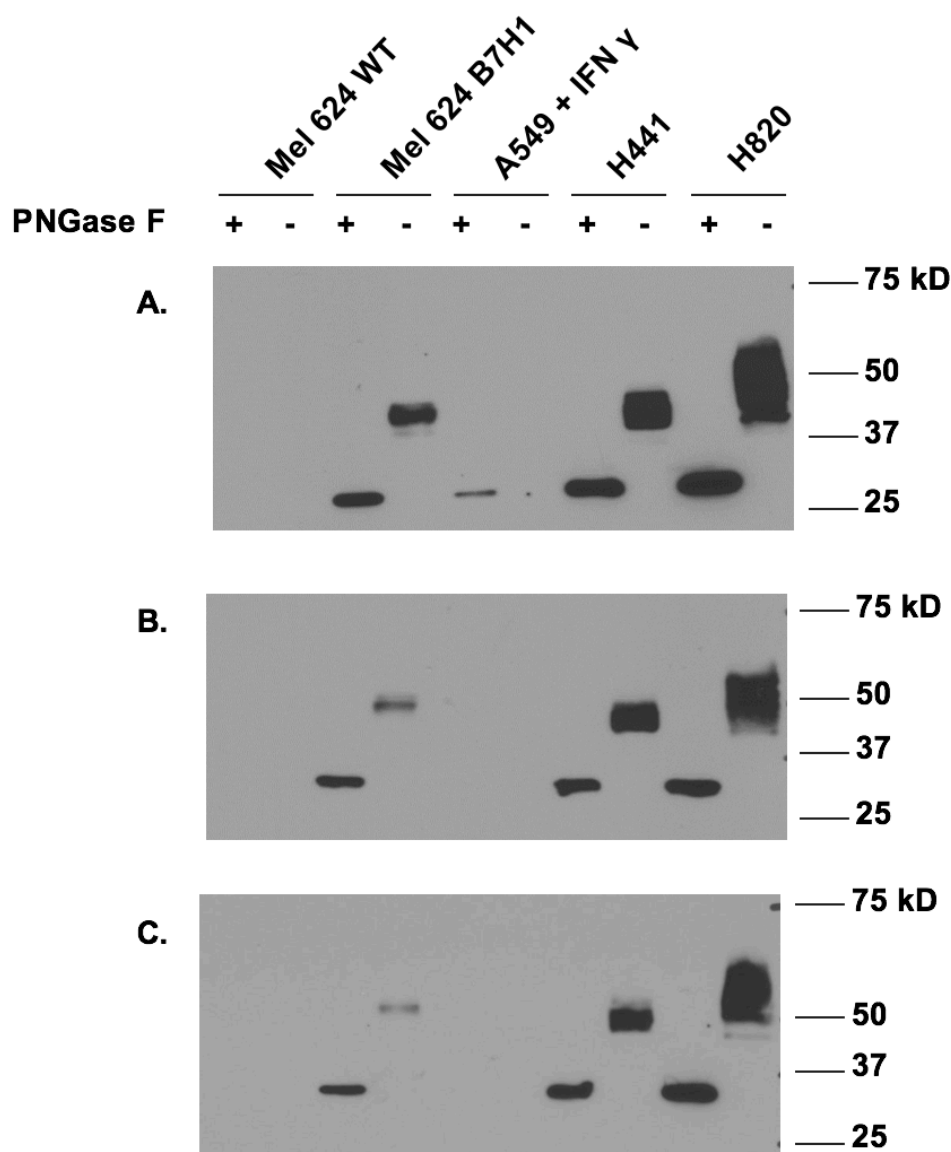
Immune activation panel as a predictive biomarker in metastatic melanoma

Of the 47 melanoma cases stained for IRF-1, 10 cases were lymph node metastases and excluded from evaluation of immune infiltrates. The remaining 37 cases were stained with a multiplex panel for CD3, Granzyme B, Ki67, DAPI, and S100/HMB45 tumor mask. Visually, tumors largely fell into one of three patterns: immune-poor (Low CD3; Figure 13A), immune-quiescent (High CD3, low Granzyme B, low Ki67; Figure 13B), or immune-active (High CD3, high Granzyme B, high Ki67; Figure 13C).

For each case, individual cells were counted and classified as positive or negative for CD3, Granzyme B, and Ki67 using the Vectra imaging platform. The number of cells per tumor, including tumor and infiltrating cells, ranged from 14,274 to 2,646,294. A higher percentage of CD3+ cells (CD3+/all cells) was associated with NRAS mutation status (Figure 14A) and CR/PR compared to SD/PD (Figure 15A, p = 0.0067), and predicted longer PFS from the start of therapy (Figure 15B, p = 0.017) when stratified by the optimal cutpoint selected for maximal effect size. Conversely, a higher percentage of CD3+ cells double-positive for CD3+ and Granzyme B+ (CD3+ Granzyme B+ / CD3+) was associated with SD/PD (Figure 15C, p = 0.023) and a trend toward inferior PFS (Figure 15D, p = 0.066). A higher percentage of CD3+ cells double positive for Ki67 and CD3 was associated with CR/PR (Figure 15E, p = 0.046), but was associated with a trend toward worse PFS from the start of therapy (Figure 15F, p = 0.079). Fractions of Granzyme B+ and Ki67+ CD3 cells were not associated with melanoma mutation status. (Figure 14B, C).

The markers were then combined to a generate a survival analysis reflecting three cohorts: immune-poor, immune-quiescent, and immune-active. When immune-rich (i.e., tumors with high numbers of CD3+ cells) cases were stratified into immune-quiescent or immune-active tumors based on the fraction of Granzyme B-positive CD3+ cells, there was a trend toward greater PFS in immune-quiescent tumors compared to both immune-poor and immune-active tumors (Figure 16A, p = 0.099). The same trend was observed when immune-active status was defined by high levels *either* Ki67 or Granzyme B positivity, though it did not reach statistical significance (Figure 16B, p = 0.23).

These analyses were then repeated with compartment-based AQUA scores in place of cell counts. CD3 signal in the DAPI compartment was higher in patients with PR/CR compared to SD/PD, though this did not reach statistical significance; likewise, there was a trend toward greater PFS in the CD3-high group (Figure 17A, B). A statistically insignificant association was observed between higher Granzyme B in the CD3+ compartment with SD/PD and inferior PFS (Figure 17 C, D). There was no appreciable difference in Ki67 signal in the CD3+ compartment between patients with PR/CR and those with SD/PD (Figure 17E); however, there was a trend toward improved PFS in the Ki-67 low group (Figure 17F).

A three-cohort survival analysis was also performed using AQUA scores as described above. Using this platform, immune-active status was associated with improved PFS, though this trend did not reach statistical significance with either definition of immune-active tumors (Figure 18 A, B).

Lastly, the correlation between cell counts as assessed with Vectra and AQUA scores was assessed for each of the three makers. The fraction of CD3+ cells positively

correlated with AQUA score for CD3 in the DAPI compartment ($R^2 = 0.50$; Figure 19A).

Likewise, the percentages of double-positive GB+ CD3+ and Ki67+ CD3+ cells

correlated with their respective AQUA scores ($R^2 = 0.58$ and R^2 0.80, respectively;

Figure 19 B, C)
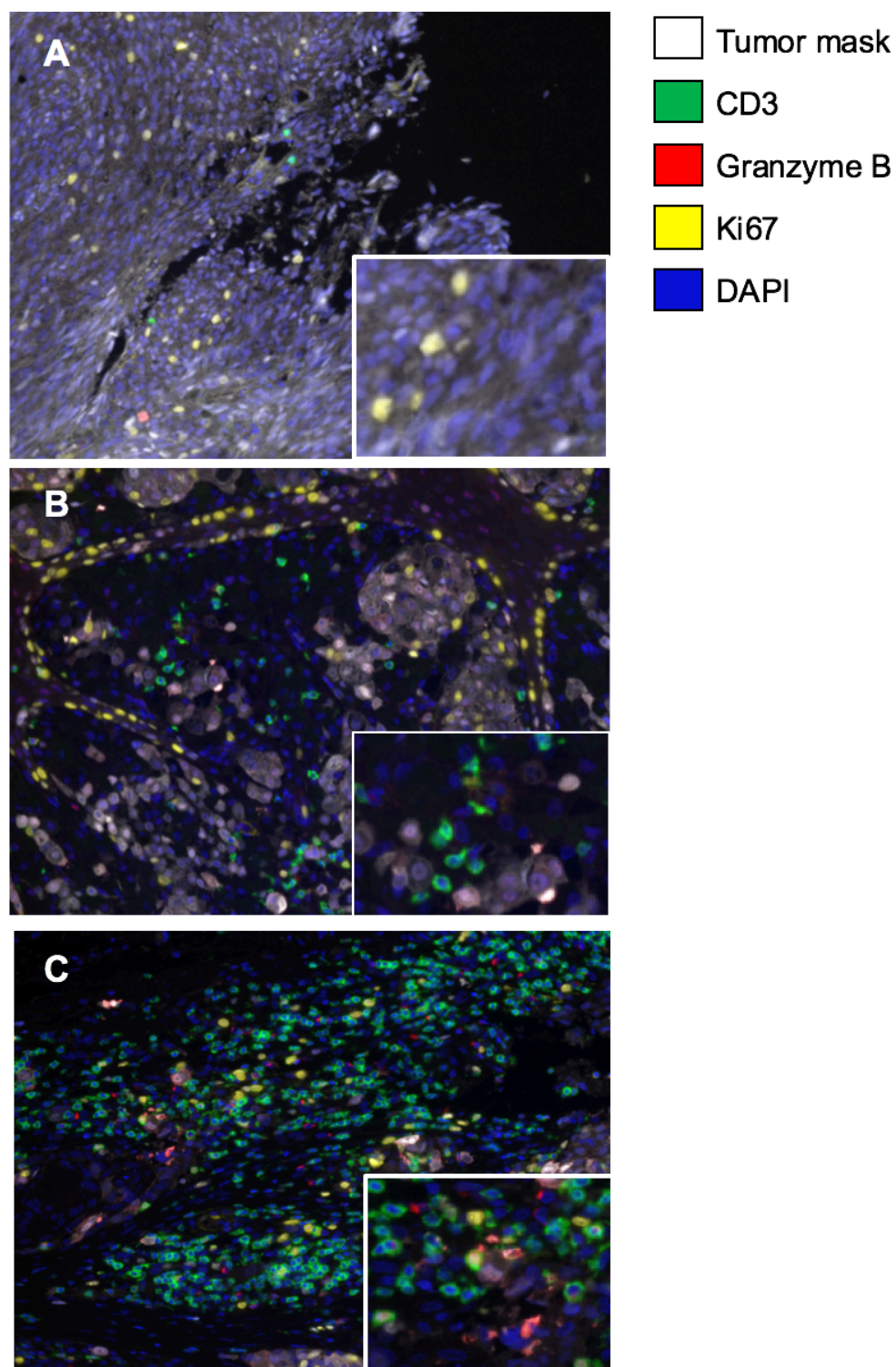
Figure 13. Representative images of melanoma cases stained for immune activation panel as captured on Vectra quantitative imaging platform. A) Immune-poor tumor with minimal CD3+ infiltrates B) Immune-quiescent tumor with CD3+ infiltrates largely negative for Granzyme B and Ki67 C) Immune-active tumor with Granzyme B+ and Ki67+ CD3+ infiltrates
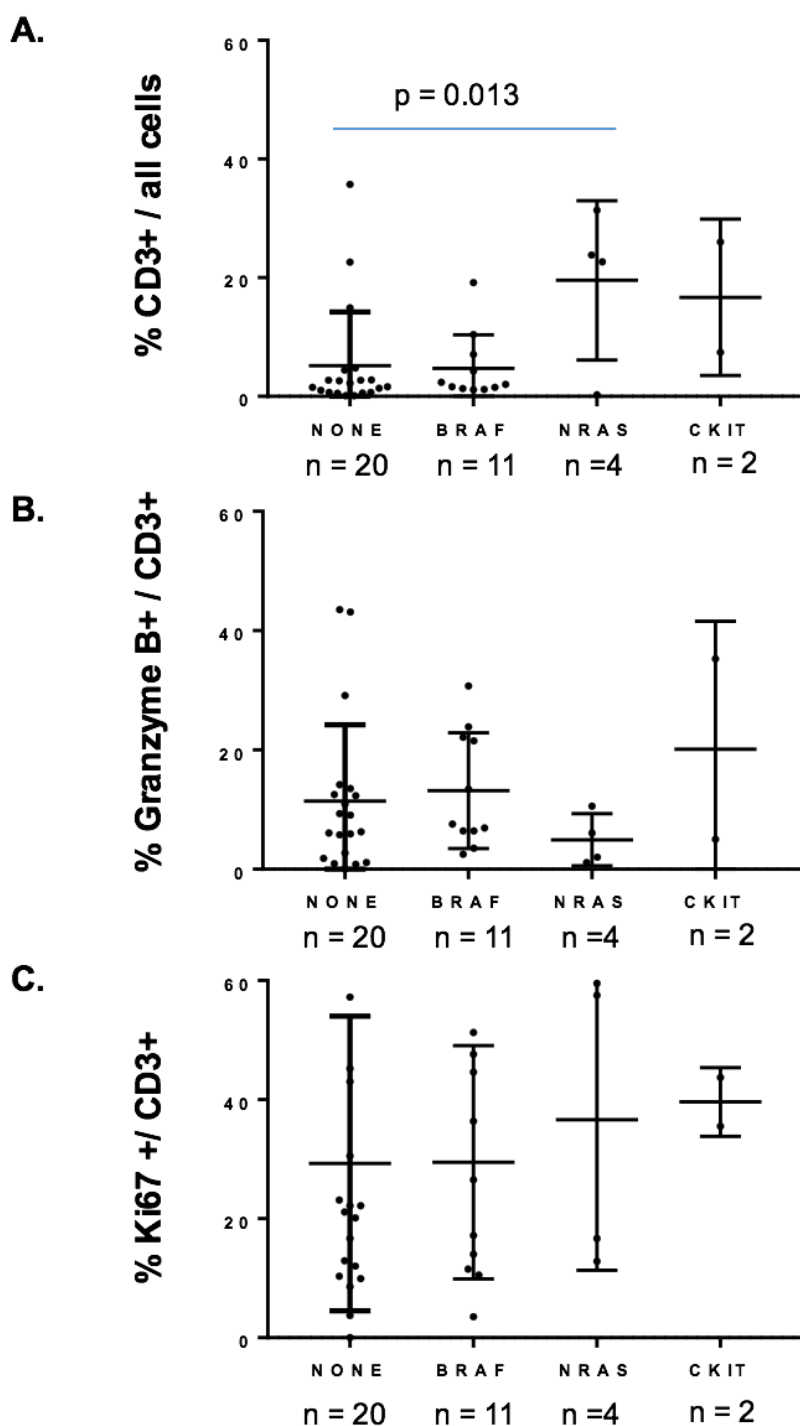
Figure 14. Immune infiltrates by melanoma mutational status as measured on Vectra platform. "None" refers to no known driver mutation identified by clinical molecular profiling. A) Percentage of all cells positive for CD3; B) Proportion of CD3+ cells positive for Granzyme B, C) Percentage of CD3+ cells positive for Ki67
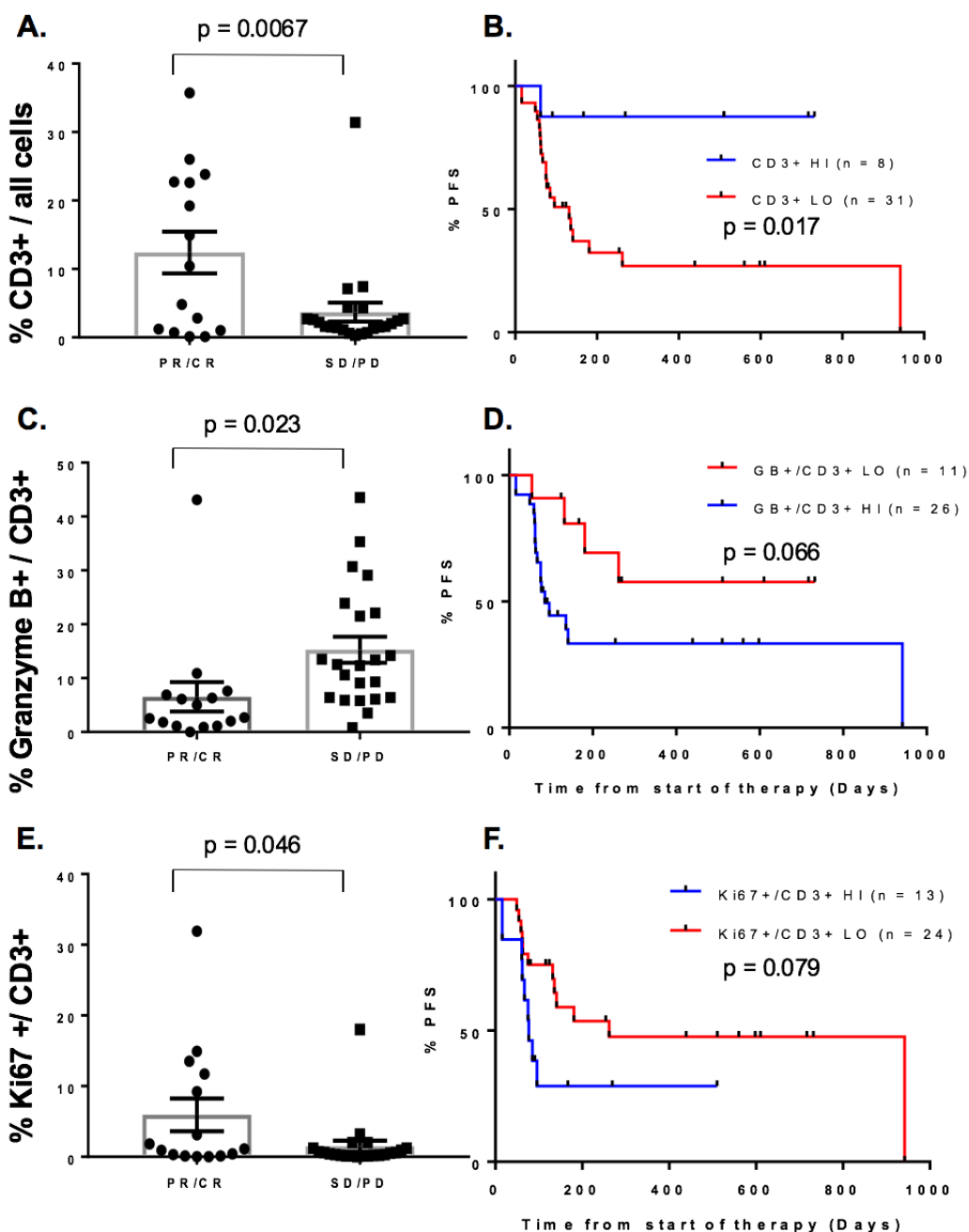
Figure 15. Univariate markers of immune activation as predictive markers for response to anti-PD-1 therapy as measured on the Vectra quantitative immunohistochemistry platform. A) ORR by % CD3+ cells B) PFS by % CD3 cells C) ORR by % Granzyme B + CD3+ cells D) PFS by % Granzyme B + CD3+ cells E) ORR by % Ki67+ CD3+ cells F)) PFS by % Ki67+ CD3+ cells

Figure 16. Integrated immune activation status as a predictive marker for PFS anti-PD-1 immunotherapy as measured by the Vectra quantitative imaging platform. A) Three-cohort survival analysis with CD3-high cohort stratified by Granzyme B expression in the CD3 compartment B) Three-cohort survival analysis with CD3-high cohort stratified by activation status, an integrated measure of either a high fraction of Granzyme B+ or Ki67+ cells in the CD3 compartment
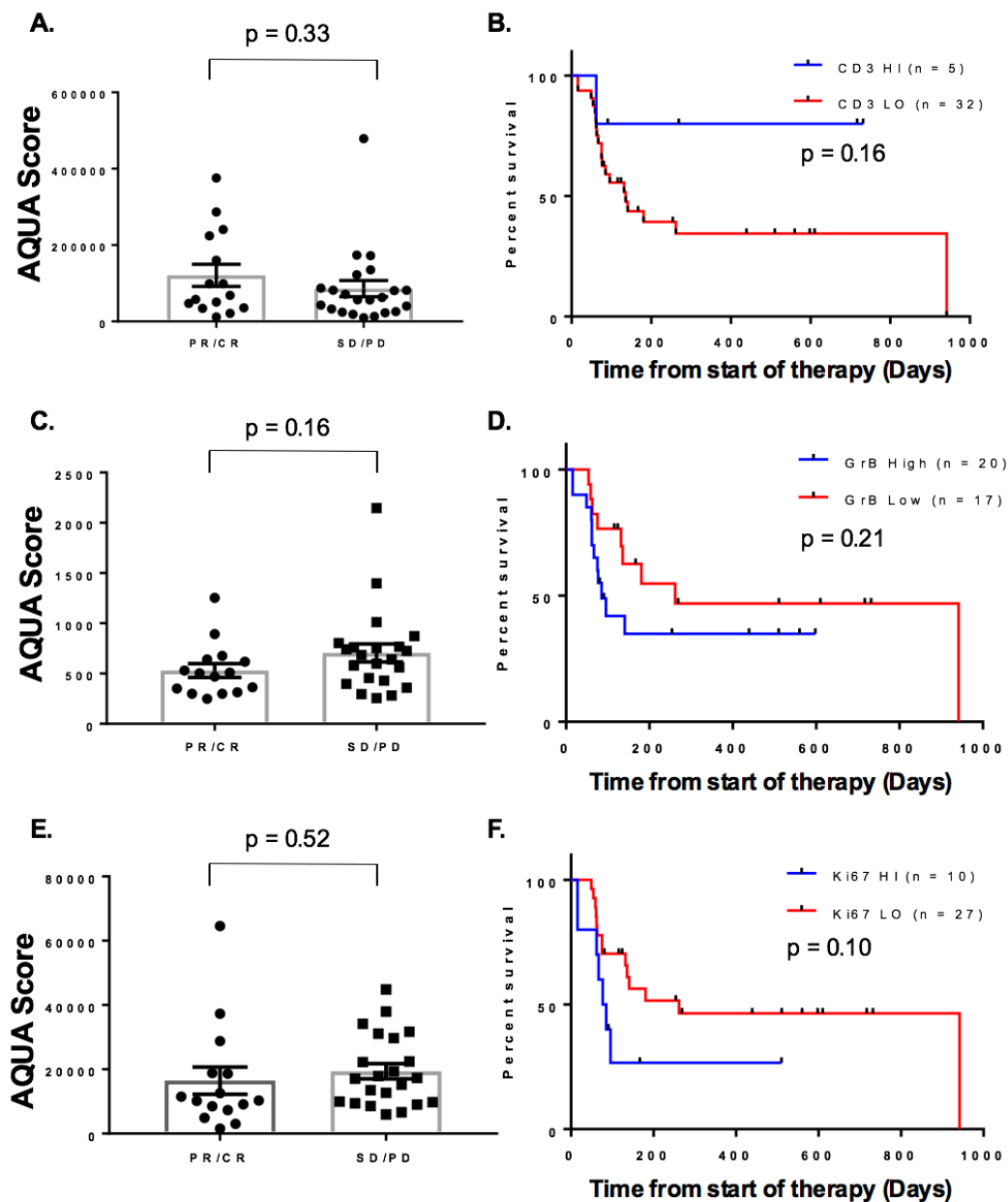
Figure 17. Univariate analyses of immune activation markers to predict response to anti-PD-1 therapy as measured by AQUA. A) ORR by CD3 measured in DAPI compartment B) PFS by CD3 measured in DAPI compartment C) ORR by Granzyme B in CD3 compartment D) PFS by Granzyme B in CD3 compartment E) ORR by Ki67 in CD3 compartment F) PFS by Ki67 in CD3 compartment
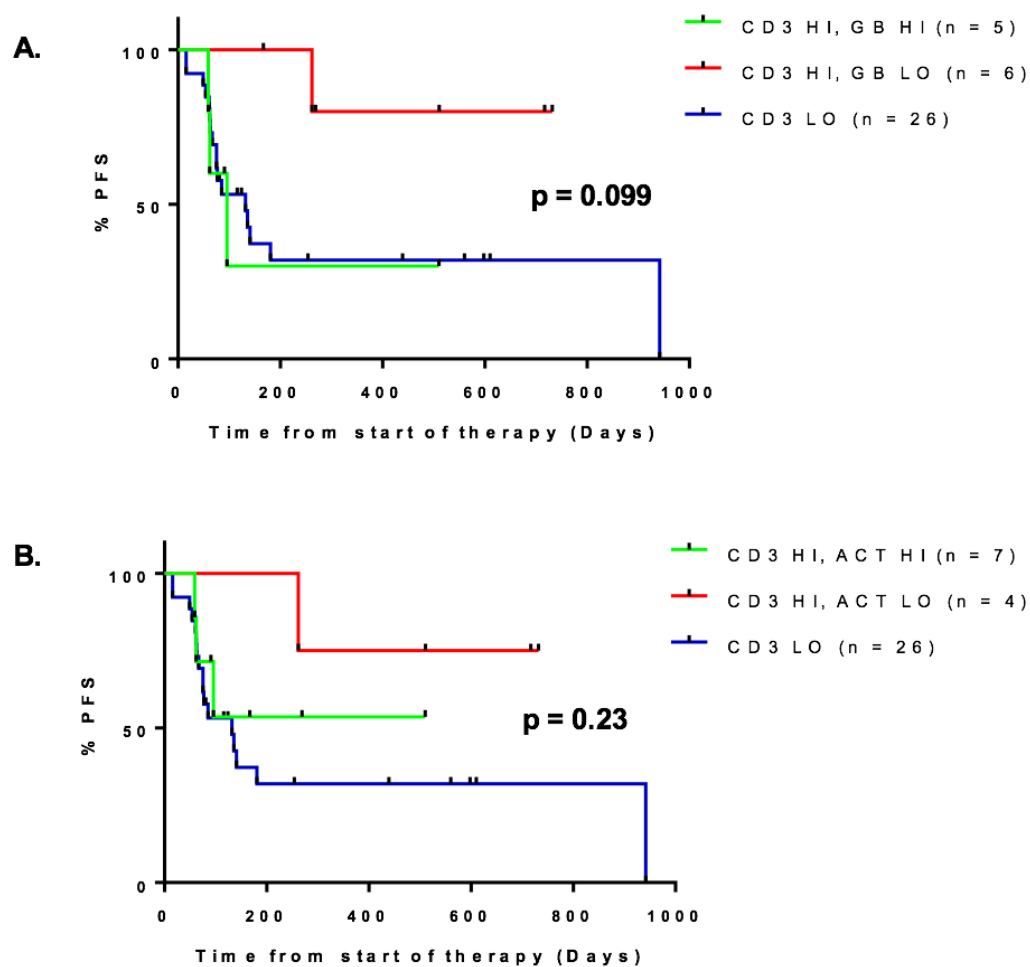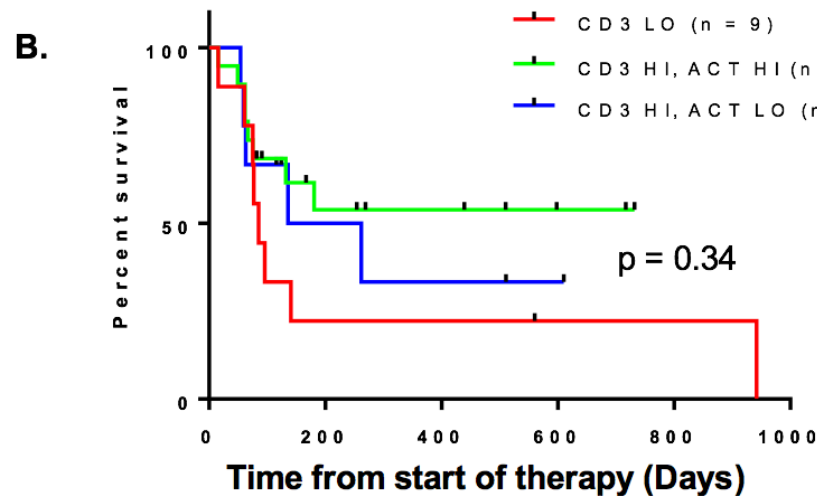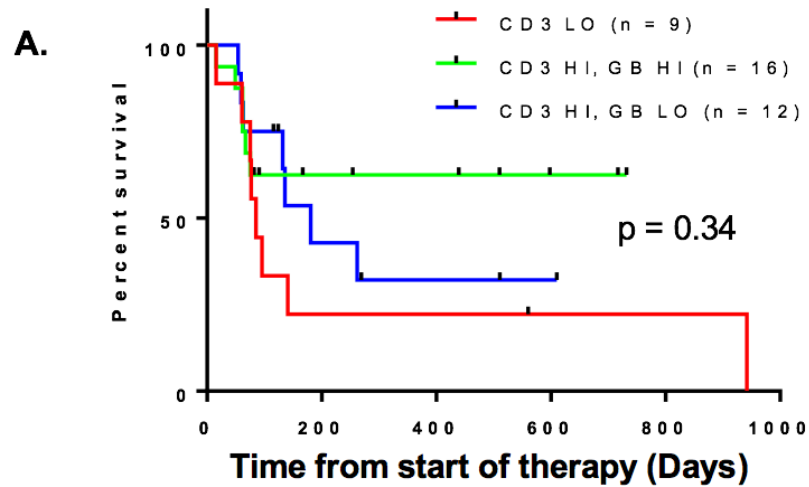
Figure 18. Integrated immune activation status as a predictive marker for PFS on anti-PD-1 immunotherapy as measured by AQUA quantitative imaging platform. A) Three-cohort survival analysis with CD3-high cohort stratified by Granzyme B (GB) expression in the CD3 compartment B) Three-cohort survival analysis with CD3-high cohort stratified by activation status (ACT), an integrated measure of either high Granzyme B or Ki67 in the CD3 compartment

A.

CD3 NORM / DAPI

$R^2 = 0.50$

B.

GB / CD3

$R^2 = 0.58$

C.

Ki67 / CD3

$R^2 = 0.80$
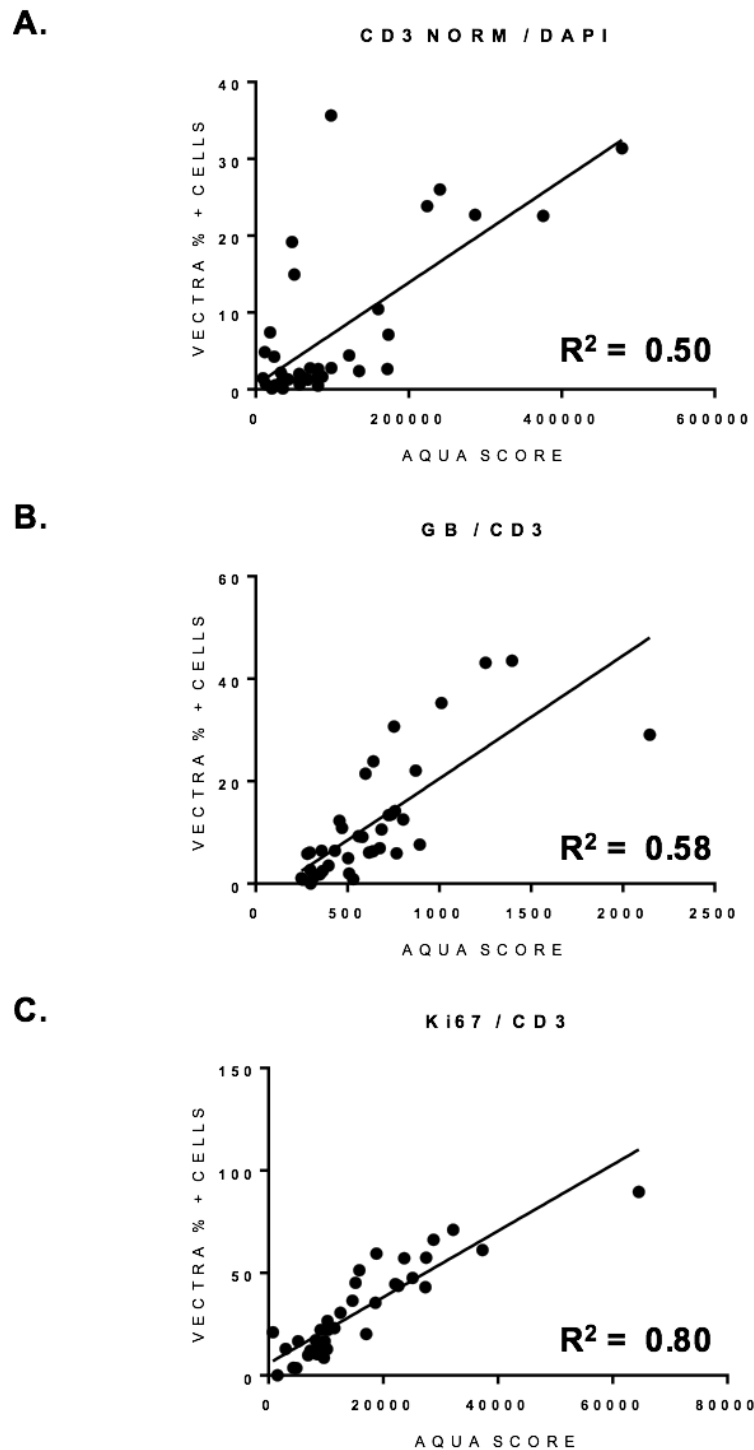
Figure 19. Comparison of immune activation markers on AQUA and Vectra platforms. A) Percentage CD3 + cells v. AQUA score of CD3 in DAPI compartment ; B) Percentage Granzyme B+ CD3 cells v. Granzyme B in CD3 compartment C) Percentage of Ki67+ CD3 cells v. Ki67 in CD3 compartment

Soluble PD-L1 in non-small cell lung cancer

Optical density and known concentrations of recombinant sPD-L1 were fit with a four-parameter logistic (4-PL) model ($R^2 = 0.9986$) to generate a standard curve (Figure 20A). Plasma samples from patients with NSCLC had significantly elevated sPD-L1 levels compared to pre-operative or post-operative age- and sex-matched controls undergoing non-oncologic surgical procedures (Figure 20B, $p < 0.0001$). Though sample size was limited, sPD-L1 was higher in samples from patients currently receiving anti-PD-1 immunotherapy compared to pre-treatment samples (Figure 20C, $p = 0.02$). In a subset analysis of pre-treatment samples, there was a trend toward higher sPD-L1 in patients that responded to anti-PD-1 immunotherapy compared to those that did not.

sPD-L1 was then assessed in plasma samples for 47 patients with known PD-L1 tissue staining status. sPD-L1 levels did not correlate with either average or maximal (i.e., highest field-of-view) PD-L1 AQUA scores for primary tumors stained with the SP142 or E1L3N (Figure 21). Additionally, sPD-L1 levels did not vary with age, sex, smoking status, histology, node status, tumor stage, or recurrence after surgery (Figure 22).

A.

B.

C.

D.
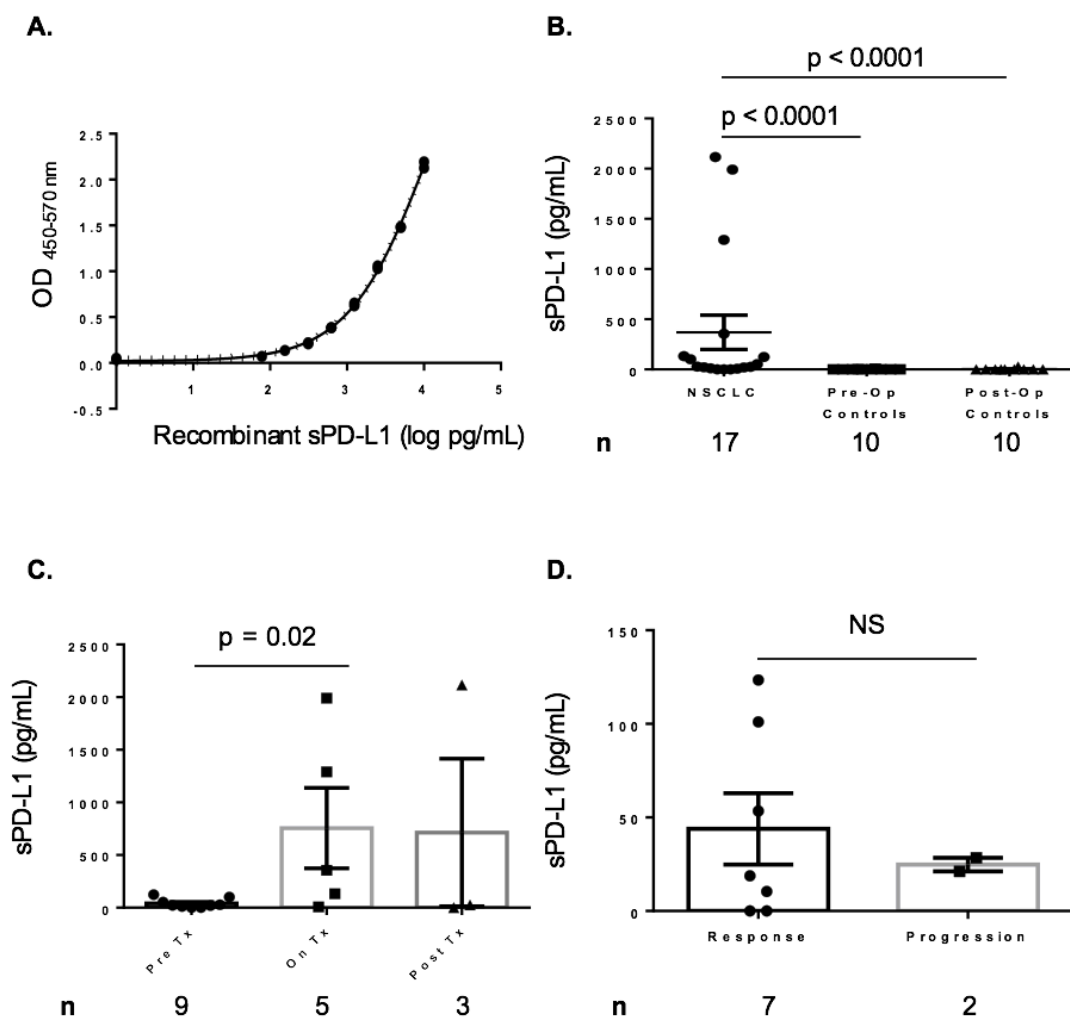
Figure 20. sPD-L1 ELISA in NSCLC cases v. cancer-free controls A) Standard curve derived from serial dilution in recombinant sPDL1 in plasma from healthy control.; B) NSCLC cases v. healthy controls; C) All specimens by sample timing relative to anti-PD-1 immunotherapy (Mean +/- SEM); D) Pre-treatment specimens by initial response (Mean +/- SEM). OD = Optical density; Tx = therapy

E1L3N **SP142**

A.

$R^2 = .0011$
p = 0.049

Average AQUA score

15000

10000

5000

0   1   2   3   4   5

B.

$R^2 = .0043$
P = 0.66

15000

10000

5000

0   1   2   3   4   5

C.

$R^2 = .0055$
p = 0.62

Max AQUA score

15000

10000

5000

0   1   2   3   4   5

sPDL1 (log pg/mL)

D.

$R^2 = .010$
P = 0.50

20000

15000

10000

5000

0   1   2   3   4   5

sPDL1 (log pg/mL)
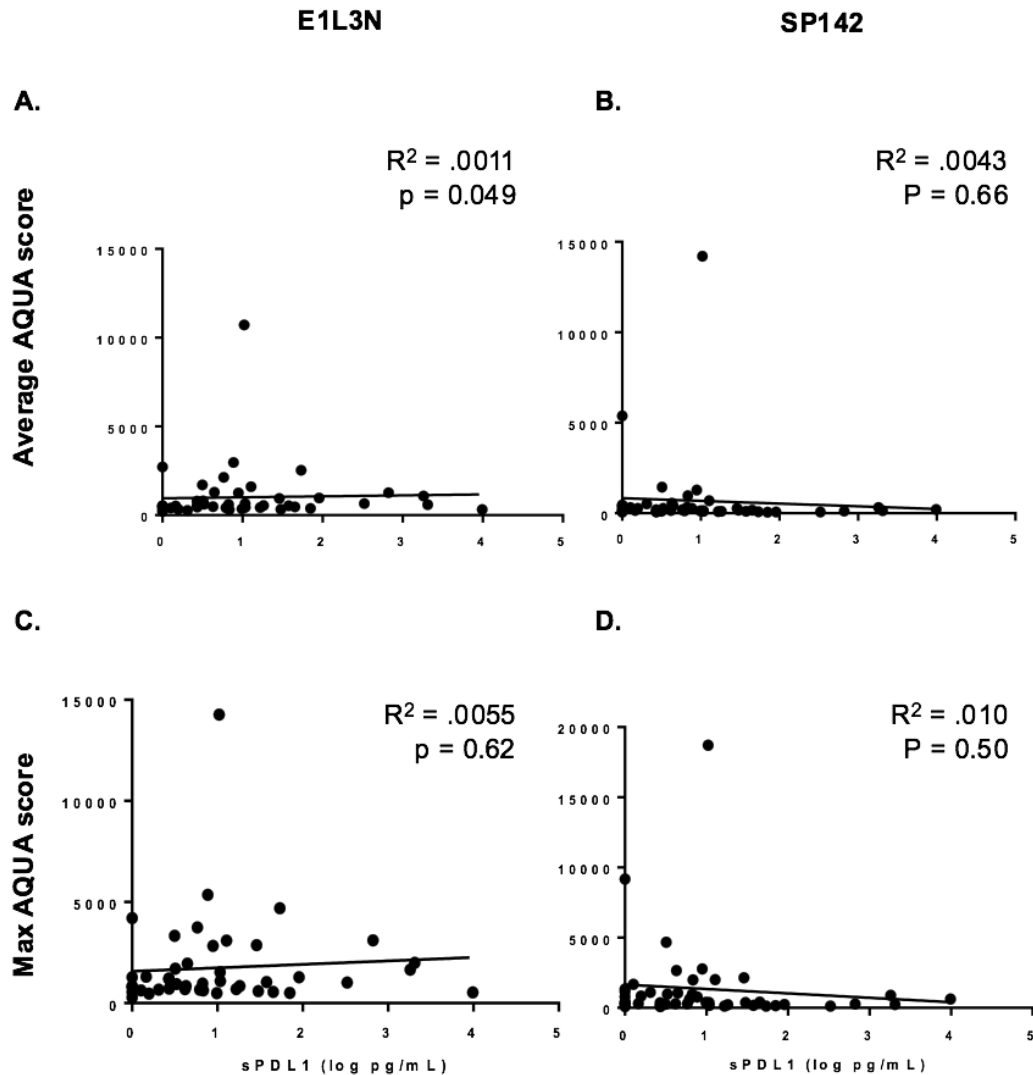
Figure 21. Correlation of plasma sPD-L1 level with tumor-based quantitative immunohistochemistry metrics in 47 NSCLC cases A) Correlation with average AQUA score of primary tumor stained with E1L3N B) Correlation with average AQUA score obtained with antibody SP142 C) Correlation with maximum FOV AQUA score obtained with antibody E1L3N D) Correlation with maximum FOV AQUA score obtained with antibody SP142
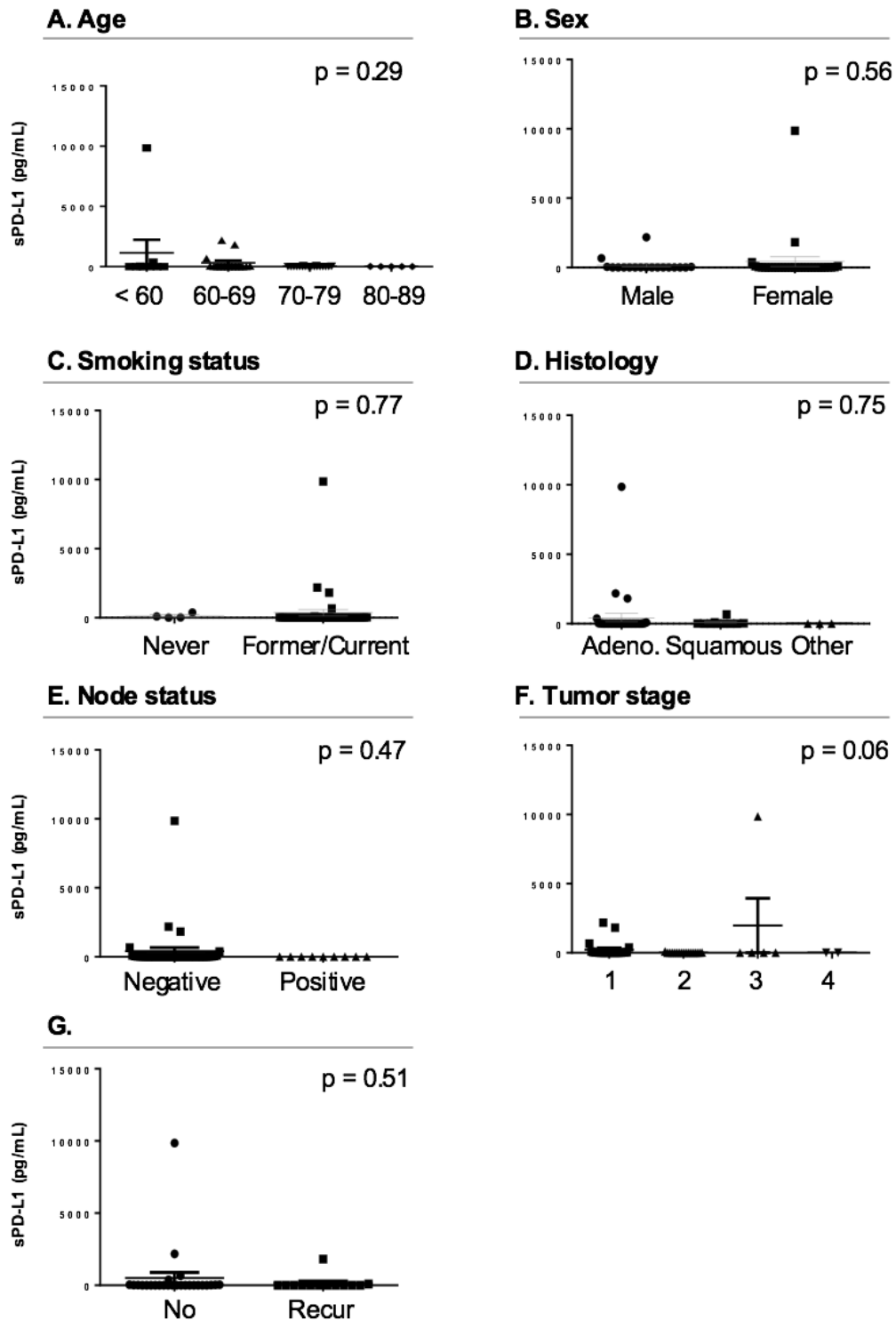
Figure 22. Correlation of sPD-L1 with clinical and pathologic variables.

V. DISCUSSION

IRF-1 as a predictive biomarker

Biomarkers for predicting response to anti-PD-1 immunotherapy have been identified as a critical unmet need in the treatment of metastatic melanoma.[65] PD-L1 has been shown to be promising in some studies[21] but not others. Here we show pilot data to suggest that capability to express PD-L1, as measured by nuclear IRF-1 expression, may be more valuable as a predictive marker than PD-L1 itself.

While IRF-1's role in regulating an inflamed melanoma phenotype has been previously characterized,[33] this is the first report of IRF-1 as a predictive tissue biomarker to anti-PD-1 immunotherapy in melanoma. Though the improved clinical responses for tumors with higher IRF-1 expression could reflect these tumors' ability to express PD-L1, this finding is also consistent with recent studies that have linked IFNγ signaling with response to PD-1[39,66-68] blockade. Given the role of IRF-1 as a mediator of IFNγ, it is also possible that IRF-1 captures a broader set of tumors suppressing immune effector cells through mechanisms other than PD-L1.

In addition to inducing PD-L1, IFNγ signaling plays a central role in inducing tumor immunogenicity through the expression of major histocompatibility complex I (MHC I).[36,37] In the pre-PD-1 era, a small study of 15 melanoma patients showed a site-specific upregulation of IRF-1 and antigen-presentation machinery in lesions responding to immunotherapies.[69] Presentation of neoantigens through MHC I may be required for ongoing response to anti-PD-1 immunotherapy, as loss of the antigen-presenting beta-two microglobulin was recently associated with acquired resistance with one patient treated

with pembrolizumab.[40] IRF-1-low tumors may have defects in antigen presentation, rendering tumors "invisible" the immune system and resistant to anti-PD-1 therapy regardless of PD-L1 expression.

Lastly, tumor expression of IRF-1 could reflect the presence of necessary T_H1 immune infiltrates in tumors with intact JAK/STAT signaling machinery. In this model, the absence of IRF-1 may be a surrogate marker of an immune-exclusionary phenotype[70] in cells that retain their ability to respond to interferon-gamma. Correlations between IRF-1, tumor-infiltrating lymphocytes, and immune-exclusionary gene signatures could help elucidate this relationship.

Though variable antibody binding to glycosylated and de-glycosylated PD-L1 was considered as one possible explanation for PD-L1's poor performance as a predictive biomarker, it appears unlikely to be a major driver of case misclassification. Treatment with PNGase F yielded narrow bands on Western blot near PD-L1's expected molecular weight of 33 kilodaltons,[22] so it is likely that N-linked glycosyl residues were effectively removed. As all three antibodies tested bound both glycosylated and deglycosylated forms, it is unlikely their respective epitopes are affected by glycosylation. This is particularly of interest for E1J2J, which is directed against an extracellular epitope--- E1L3N and SP142 are antibodies directed against the intracellular domain of PD-L1, which does not have any N-linked glycosylation sites.

To further illustrate the clinical relevance of PD-L1 glycosylation, it would be informative to repeat this experiment with antibodies from the FDA-approved IHC assays for PD-L1. Also, as the conditions for antigen binding are markedly different on a Western blot compared to FFPE tissue, it would also be useful to perform *in situ*

deglycosylation on tumor samples and compare the efficacy of several antibodies in this setting. However, initial attempts to deglycosylate proteins with PNGase F in FFPE did not yield reproducible results. Further optimization of this protocol would help to determine whether glycosylation status has an effect on the performance of a given IHC assay.

There are a number of limitations to consider for this pilot biomarker study comparing IRF-1 and PD-L1. Perhaps the most significant is the small samples size and the fact that the study is a single institutional, retrospective analysis. Another potential issue is the selection of a cutpoint to distinguish high from low expressers for an assay that results in a continuous data set. Here, we sought to bolster the lowest-tertile cutpoint by also using the limit of detection in unstimulated melanoma cell lines. Using this alternate cutpoint, only three cases were re-classified from the low-IRF-1 to the high-IRF-1 group, and the difference in PFS between IRF-1-high and IRF-1-low patients remained significant. Further development of IRF-1 as a predictive biomarker will require validation of an optimal, reproducibly defined, cutpoint on additional cohorts, as well as inclusion in prospective studies. Also, as the study cohort included patients treated with both single-agent PD-1 and combination PD-1/CTLA-4 blockade, future studies should likely be limited to a more uniform treatment strategy.

While the underlying mechanisms remain unclear, there are a number of biological explanations that could explain the association between IRF-1 expression and response to anti-PD-1 immunotherapy. With further validation, it is possible that an IHC-based assay for IRF-1 could be readily transferred to the clinical setting. The concept of a companion diagnostic tested based on capability to express the target of PD-1 axis

therapy may address some of the current assays deficiencies related to heterogeneity or other less well defined variables.

Immune activation as a predictive biomarker

In addition to IRF-1, a multiplex immune activation panel was also evaluated as a biomarker to predict response to anti-PD-1 immunotherapy. This panel has been previously shown to be predictive of response in a discovery cohort of treated NSCLC, but has yet to be applied to melanoma (Schalper et al., manuscript in review).

Reassuringly, higher proportions of CD3+ cells were predictive of both ORR as well as PFS. This observation is aligned with previous reports of the importance of T cell infiltrates in the response to anti-PD-1 immunotherapy, and suggests that this assay effectively quantitates T cell infiltrates. Notably, as CD3 is a pan-T cell marker, it remains unknown whether response depends on pre-existing CD4+ or CD8+ infiltrates. Previous attempts to quantitate the CD8+ population have been largely limited by difficulty in accurately assessing signals that represent low fraction of total tumor area (i.e., < 5%). More granular assessment of immune cell populations infiltrating pre-treatment and on-treatment tumor samples will likely provide more specific predictions of response and further insights into the mechanisms underlying tumor destruction after PD-1 blockade.

In addition to overall CD3+ counts, this assay also provides insight into their functional status via colocalization of CD3 with Ki67 and Granymze B. Within the immune compartment, the ratio of double-positive Granzyme B+ CD3+ cells to CD3+ cells also predicted ORR, with lower levels of Granzyme B associated with greater

clinical benefit. This observation may reflect that a population of quiescent CD3+ cells is required for an active anti-tumor response with the release of PD-1-mediated inhibition. Conversely, in tumors with active immune infiltrates, (CD3-high, Granzyme B-high), blockade of PD-1 may not further potentiate immune response. If these immune-active tumors are indeed subjected to ongoing cytolytic activity, and yet are not adequately controlled by the host immune system, it is possible that these tumors have developed alternative mechanisms of resistance from cytotoxic components that warrant further investigation. For example, a recent analysis of genomic data from The Cancer Genome Atlas showed that cytolytic activity was associated with mutations in antigen-presenting machinery, including beta-2-microglobulin, HLA-A, HLA-B, and HLA-C.[71]

Few comparable data are available on immune activation as a predictor of response—one small study 13 patients found mRNA levels of Granzyme A, but not Granzyme B, higher in pre-treatment tumor specimens of responders than non-responders.[72]

The role of CD3+ cell proliferation as measured by Ki67 remains unclear—a higher percentage of Ki67+ CD3 cells was associated with PR/CR, but also trended toward inferior PFS. While Ki67 may represent an activated T cells, it is also possible that dysfunctional T cells may proliferate. Multiplex staining with immune inhibitory receptors such as PD-1 may elucidate whether proliferating T cells are likely to be functional.

A three-cohort survival analysis distinguishing immune-poor (CD3-low), immune-active (CD3-high, GB-high +/- Ki67-high) and immune-quiescent (CD3-high, GB-low +/- Ki67-low) was also performed to mirror the analysis performed by Schalper

and colleagues. On the Vectra platform, the results trended toward what had been observed in NSCLC—the immune-quiescent tumors had the best PFS. However, the analysis of 37 melanoma tumors did not reach statistical significance.

This retrospective study was underpowered with only 37 cases, and it is possible that the inclusion of additional cases would further resolve survival differences between immune-poor, immune-active, and immune-quiescent tumors. A formal power analysis was not performed as all available samples at Yale were used in for this study. This cohort also contained more heterogeneity than the NSCLC cohort under study—while the NSCLC cases were exclusively treated with single-agent anti-PD-1 therapy (e.g., nivolumab or pembrolizumab), a significant portion of the melanoma cohort was treated with combination therapy of ipilimumab and nivolumab. It is plausible, but speculative, that the blockade of CTLA-4 may alter the immune activation status of a given tumor and change its susceptibility to PD-1 blockade.

Alternatively, melanomas may be less heterogeneous than NSCLC in the degree of immune infiltration, so it is more difficult to identify an immune-poor cohort of tumors. The three-cohort PFS analysis is contingent on the setting of two or three cut-points to delineate the high- and low-expressing cohorts for each marker. In this study, as well as that of NSCLC, these limits were empirically. It is possible that the selected cutpoints do not reflect meaningful differences in underlying tumor biology. Further validation of this assay would require prospectively selected cut-points, based either on biologic rationales or on these initial observations

Capturing the same slides with both the AQUA and Vectra quantitative immunohistochemistry systems afforded an opportunity to compare these two imaging

platforms. While AQUA calculates scores based on the cumulative signal intensity of a given target in a pre-specified mask (e.g., all CD3+ areas), the inForm software for Vectra leverages a user-trained machine learning algorithm to segment individual cells and phenotype them as positive or negative for each marker of interest. These techniques represent fundamentally different ways of quantifying immunoflurorescent signal—while AQUA provides an objective target score, its accuracy has historically been limited when the mask area takes up a low percentage (i.e., less than 2-5%) of a field of view. In contrast, the Vectra platform relies on user input to define cell and tissue compartments. While this has raised concerns as to its run-to-run reproducibility, early studies have suggested that it may be better suited for detecting low-frequency events. This feature could be useful in characterizing immune infiltrates, which often take up a relatively small fraction of tumor area. The previous study of the activation panel assay in NSCLC by Schalper et al. solely leveraged the AQUA platform.

Univariate analyses of CD3 infiltrates and Granzyme B positivity in CD3+ cells were more predictive when captured on the Vectra than on AQUA. Of the three markers, the correlation between AQUA and Vectra was also the poorest for CD3+ ($R^2 = 0.50$). This suggests that cell counting may be a more viable method that compartment-based quantification for characterizing immune infiltrates. In future studies, is possible that Vectra may be able to overcome the limitations of low signal area and more accurately evaluate rare populations of infiltrating immune cells.

In sum, while the combined three-cohort immune activation assay of CD3, Ki67, and Granzyme B did not predict PFS as previously observed in NSCLC, there was a similar trend toward better survival in the immune-quiescent panel when assessed by the

Vectra imaging system. Furthermore, the individual markers of CD3+ cell fraction and Granzyme B+ CD3+ / CD3+ cell fraction were associated with meaningful differences in ORR and PFS. The evaluation of more treated melanoma cases with this technique will help to clarify how this assay can best be used to predict response to anti-PD-1 immunotherapy.

Pilot studies of sPD-L1 in NSCLC

In addition to comparing tissue-based markers, a pilot study was completed toward developing a clinically applicable plasma-based assay for soluble PD-L1. Due to the unavailability of plasma from metastatic melanoma patients, plasma sPD-L1 levels in NSCLC patients were compared to those of age- and smoking-matched controls using a commercially available non-clinical PD-L1 ELISA kit. The tightly fitted standard control curve with known quantities of recombinant sPD-L1 in control plasma suggests that the optical signal from this assay accurately reflects sPD-L1 levels. Furthermore, initial analyses confirmed prior reports that sPD-L1 levels are elevated in NSCLC compared to cancer-free controls.[58] As sPD-L1 levels were largely undetectable in cancer free both pre-operatively and two days after general surgery, it appears that sPD-L1 is not elevated in this nonspecific inflammatory state. Further testing of other inflammatory conditions, including autoimmune disease, is warranted to determine if sPD-L1 is specific to oncologic diagnoses.

Initial results comparing sPD-L1's relationship to anti-PD-1 therapy are provocative, but extremely limited by small sample size. Namely, a subset analysis

demonstrated sPD-L1 may be higher in on-treatment samples compared to pre-treatment samples, and that there was an insignificant trend toward higher expression in pre-treatment samples of responders compared to non-responders. Future studies in NSCLC and melanoma should draw from larger cohorts of pre-treatment and on-treatment plasmas samples, so that sPD-L1 can be thoroughly evaluated as a means to predict response to treatment and track response to therapy over time in responders and non-responders. Ideally, plasma from clinical trial patients could be accessed for the best-controlled evaluation of clinical endpoints.

Given these promising initial results, the ELISA technique evaluated could likely be applied to larger cohorts of patients treated with anti-PD-1 therapy to generate clinically relevant data about sPD-L1 as a predictive biomarker.

References

1. Hanahan D, Weinberg RA. Hallmarks of cancer: the next generation. Cell 2011;144:646-74.

2. Pardoll DM. The blockade of immune checkpoints in cancer immunotherapy. Nat Rev Cancer 2012;12:252-64.

3. Rudd CE, Taylor A, Schneider H. CD28 and CTLA-4 coreceptor expression and signal transduction. Immunol Rev 2009;229:12-26.

4. van der Merwe PA, Bodian DL, Daenke S, Linsley P, Davis SJ. CD80 (B7-1) binds both CD28 and CTLA-4 with a low affinity and very fast kinetics. J Exp Med 1997;185:393-403.

5. Hodi FS, O'Day SJ, McDermott DF, et al. Improved survival with ipilimumab in patients with metastatic melanoma. N Engl J Med 2010;363:711-23.

6. Schats KA, Van Vre EA, De Schepper S, et al. Validated PD-L1 immunohistochemistry assays (E1L3N & SP142) reveal similar immune cell staining patterns in melanoma when using the same sensitive detection system. Histopathology 2016.

7. Dong H, Strome SE, Salomao DR, et al. Tumor-associated B7-H1 promotes T-cell apoptosis: a potential mechanism of immune evasion. Nat Med 2002;8:793-800.

8. Freeman GJ, Long AJ, Iwai Y, et al. Engagement of the PD-1 immunoinhibitory receptor by a novel B7 family member leads to negative regulation of lymphocyte activation. J Exp Med 2000;192:1027-34.

9. Amarnath S, Mangus CW, Wang JC, et al. The PDL1-PD1 axis converts human TH1 cells into regulatory T cells. Sci Transl Med 2011;3:111ra20.

10. Habicht A, Dada S, Jurewicz M, et al. A link between PDL1 and T regulatory cells in fetomaternal tolerance. J Immunol 2007;179:5211-9.

11. Park HJ, Park JS, Jeong YH, et al. PD-1 upregulated on regulatory T cells during chronic virus infection enhances the suppression of CD8+ T cell immune response via the interaction with PD-L1 expressed on CD8+ T cells. J Immunol 2015;194:5801-11.

12. Topalian SL, Hodi FS, Brahmer JR, et al. Safety, activity, and immune correlates of anti-PD-1 antibody in cancer. N Engl J Med 2012;366:2443-54.

13. Robert C, Long GV, Brady B, et al. Nivolumab in previously untreated melanoma without BRAF mutation. N Engl J Med 2015;372:320-30.

14. Larkin J, Lao CD, Urba WJ, et al. Efficacy and Safety of Nivolumab in Patients With BRAF V600 Mutant and BRAF Wild-Type Advanced Melanoma: A Pooled Analysis of 4 Clinical Trials. JAMA Oncol 2015;1:433-40.

15. Hodi FS, Kluger H, Sznol M, et al. Durable, long-term survival in previously treated patients with advanced melanoma (MEL) who received nivolumab (NIVO) monotherapy in a phase I trial. AACR Annual Meeting 2016; 2016 April 16-20, 2016; New Orleans, LA; 2016.

16. Robert C, Schachter J, Long GV, et al. Pembrolizumab versus Ipilimumab in Advanced Melanoma. N Engl J Med 2015;372:2521-32.

17. Ribas A, Hamid O, Daud A, et al. Association of Pembrolizumab With Tumor Response and Survival Among Patients With Advanced Melanoma. JAMA 2016;315:1600-9.

18. Larkin J, Hodi FS, Wolchok JD. Combined Nivolumab and Ipilimumab or Monotherapy in Untreated Melanoma. N Engl J Med 2015;373:1270-1.

19. D'Angelo SP, Larkin J, Sosman JA, et al. Efficacy and Safety of Nivolumab Alone or in Combination With Ipilimumab in Patients With Mucosal Melanoma: A Pooled Analysis. J Clin Oncol 2017;35:226-35.

20. Weber JS, Gibney G, Sullivan RJ, et al. Sequential administration of nivolumab and ipilimumab with a planned switch in patients with advanced melanoma (CheckMate 064): an open-label, randomised, phase 2 trial. Lancet Oncol 2016;17:943-55.

21. Daud AI, Wolchok JD, Robert C, et al. Programmed Death-Ligand 1 Expression and Response to the Anti–Programmed Death 1 Antibody Pembrolizumab in Melanoma. Journal of Clinical Oncology 2016;Published online before print

22. Dong H, Zhu G, Tamada K, Chen L. B7-H1, a third member of the B7 family, co-stimulates T-cell proliferation and interleukin-10 secretion. Nat Med 1999;5:1365-9.

23. Li D, Zhang P, Li F, et al. Recognition of N-glycoforms in human chorionic gonadotropin by monoclonal antibodies and their interaction motifs. J Biol Chem 2015.

24. Li X, Qian H, Takizawa M, et al. N-linked glycosylation on laminin gamma1 influences recognition of anti-laminin gamma1 pemphigoid autoantibodies. J Dermatol Sci 2015;77:125-9.

25. Fernsten PD, Czyzyk JK, Mimura T, Winfield JB. Carbohydrate specificity of IgM autoantibodies to CD45 in systemic lupus erythematosus. Mol Biol Rep 1994;20:85-95.

26. McLaughlin J, Han G, Schalper KA, et al. Quantitative Assessment of the Heterogeneity of PD-L1 Expression in Non-Small-Cell Lung Cancer. JAMA Oncol 2016;2:46-54.

27. Taube JM, Anders RA, Young GD, et al. Colocalization of inflammatory response with B7-h1 expression in human melanocytic lesions supports an adaptive resistance mechanism of immune escape. Sci Transl Med 2012;4:127ra37.

28. Kluger HM, Zito CR, Barr ML, et al. Characterization of PD-L1 Expression and Associated T-cell Infiltrates in Metastatic Melanoma Samples from Variable Anatomic Sites. Clin Cancer Res 2015;21:3052-60.

29. Darnell JE, Jr., Kerr IM, Stark GR. Jak-STAT pathways and transcriptional activation in response to IFNs and other extracellular signaling proteins. Science 1994;264:1415-21.

30. Lee SJ, Jang BC, Lee SW, et al. Interferon regulatory factor-1 is prerequisite to the constitutive expression and IFN-gamma-induced upregulation of B7-H1 (CD274). FEBS Lett 2006;580:755-62.

31. Tumeh PC, Harview CL, Yearley JH, et al. PD-1 blockade induces responses by inhibiting adaptive immune resistance. Nature 2014;515:568-71.

32. Abiko K, Matsumura N, Hamanishi J, et al. IFN-gamma from lymphocytes induces PD-L1 expression and promotes progression of ovarian cancer. Br J Cancer 2015;112:1501-9.

33. Ascierto ML, De Giorgi V, Liu Q, et al. An immunologic portrait of cancer. J Transl Med 2011;9:146.

34. Zaidi MR, Merlino G. The two faces of interferon-gamma in cancer. Clin Cancer Res 2011;17:6118-24.

35. Farrar MA, Fernandez-Luna J, Schreiber RD. Identification of two regions within the cytoplasmic domain of the human interferon-gamma receptor required for function. J Biol Chem 1991;266:19626-35.

36. Kaplan DH, Shankaran V, Dighe AS, et al. Demonstration of an interferon gamma-dependent tumor surveillance system in immunocompetent mice. Proc Natl Acad Sci U S A 1998;95:7556-61.

37. Dighe AS, Richards E, Old LJ, Schreiber RD. Enhanced in vivo growth and resistance to rejection of tumor cells expressing dominant negative IFN gamma receptors. Immunity 1994;1:447-56.

38. Shankaran V, Ikeda H, Bruce AT, et al. IFNgamma and lymphocytes prevent primary tumour development and shape tumour immunogenicity. Nature 2001;410:1107-11.

39. Ribas A, Robert C, Hodi F, et al. Association of response to programmed death receptor 1 (PD-1) blockade with pembrolizumab (MK-3475) with an interferon-inflammatory immune gene signature. Journal of Clinical Oncology 2015;33.

40. Zaretsky JM, Garcia-Diaz A, Shin DS, et al. Mutations Associated with Acquired Resistance to PD-1 Blockade in Melanoma. N Engl J Med 2016.

41. Shin DS, Zaretsky JM, Escuin-Ordinas H, et al. Primary Resistance to PD-1 Blockade Mediated by JAK1/2 Mutations. Cancer Discov 2016.

42. Tamura T, Yanai H, Savitsky D, Taniguchi T. The IRF family transcription factors in immunity and oncogenesis. Annu Rev Immunol 2008;26:535-84.

43. Nozawa H, Oda E, Ueda S, et al. Functionally inactivating point mutation in the tumor-suppressor IRF-1 gene identified in human gastric cancer. Int J Cancer 1998;77:522-7.

44. Murtas D, Maric D, De Giorgi V, et al. IRF-1 responsiveness to IFN-gamma predicts different cancer immune phenotypes. Br J Cancer 2013;109:76-82.

45. Lim SO, Li CW, Xia W, et al. Deubiquitination and Stabilization of PD-L1 by CSN5. Cancer Cell 2016.

46. Song M, Chen D, Lu B, et al. PTEN loss increases PD-L1 protein expression and affects the correlation between PD-L1 expression and clinical parameters in colorectal cancer. PLoS One 2013;8:e65821.

47. Xu C, Fillmore CM, Koyama S, et al. Loss of Lkb1 and Pten leads to lung squamous cell carcinoma with elevated PD-L1 expression. Cancer Cell 2014;25:590-604.

48. Lastwika KJ, Wilson W, 3rd, Li QK, et al. Control of PD-L1 Expression by Oncogenic Activation of the AKT-mTOR Pathway in Non-Small Cell Lung Cancer. Cancer Res 2016;76:227-38.

49. Concha-Benavente F, Srivastava RM, Trivedi S, et al. Identification of the Cell-Intrinsic and -Extrinsic Pathways Downstream of EGFR and IFNgamma That Induce PD-L1 Expression in Head and Neck Cancer. Cancer Res 2016;76:1031-43.

50. Cochran AJ. Histology and prognosis in malignant melanoma. J Pathol 1969;97:459-68.

51. Clemente CG, Mihm MC, Jr., Bufalino R, Zurrida S, Collini P, Cascinelli N. Prognostic value of tumor infiltrating lymphocytes in the vertical growth phase of primary cutaneous melanoma. Cancer 1996;77:1303-10.

52. Spranger S, Spaapen RM, Zha Y, et al. Up-regulation of PD-L1, IDO, and T(regs) in the melanoma tumor microenvironment is driven by CD8(+) T cells. Sci Transl Med 2013;5:200ra116.

53. Schwaederle M, Husain H, Fanta PT, et al. Use of Liquid Biopsies in Clinical Oncology: Pilot Experience in 168 Patients. Clin Cancer Res 2016.

54. Sacher AG, Paweletz C, Dahlberg SE, et al. Prospective Validation of Rapid Plasma Genotyping for the Detection of EGFR and KRAS Mutations in Advanced Lung Cancer. JAMA Oncol 2016;2:1014-22.

55. Kakoulidou M, Giscombe R, Zhao X, Lefvert AK, Wang X. Human Soluble CD80 is generated by alternative splicing, and recombinant soluble CD80 binds to CD28 and CD152 influencing T-cell activation. Scand J Immunol 2007;66:529-37.

56. Frigola X, Inman BA, Lohse CM, et al. Identification of a soluble form of B7-H1 that retains immunosuppressive activity and is associated with aggressive renal cell carcinoma. Clin Cancer Res 2011;17:1915-23.

57. Rossille D, Gressier M, Damotte D, et al. High level of soluble programmed cell death ligand 1 in blood impacts overall survival in aggressive diffuse large B-Cell lymphoma: results from a French multicenter clinical trial. Leukemia 2014;28:2367-75.

58. Cheng S, Zheng J, Zhu J, et al. PD-L1 gene polymorphism and high level of plasma soluble PD-L1 protein may be associated with non-small cell lung cancer. Int J Biol Markers 2015;30:e364-8.

59. Uhlen M, Bandrowski A, Carr S, et al. A proposal for validation of antibodies. Nat Methods 2016;13:823-7.

60. Eisenhauer EA, Therasse P, Bogaerts J, et al. New response evaluation criteria in solid tumours: revised RECIST guideline (version 1.1). Eur J Cancer 2009;45:228-47.

61. Chiou VL, Burotto M. Pseudoprogression and Immune-Related Response in Solid Tumors. J Clin Oncol 2015;33:3541-3.

62. Wimberly H, Brown JR, Schalper K, et al. PD-L1 Expression Correlates with Tumor-Infiltrating Lymphocytes and Response to Neoadjuvant Chemotherapy in Breast Cancer. Cancer Immunol Res 2014.

63. Camp RL, Chung GG, Rimm DL. Automated subcellular localization and quantification of protein expression in tissue microarrays. Nat Med 2002;8:1323-7.

64. Brown JR, Wimberly H, Lannin DR, Nixon C, Rimm DL, Bossuyt V. Multiplexed quantitative analysis of CD3, CD8, and CD20 predicts response to neoadjuvant chemotherapy in breast cancer. Clin Cancer Res 2014;20:5995-6005.

65. Buchbinder EI, Hodi FS. Melanoma in 2015: Immune-checkpoint blockade - durable cancer control. Nat Rev Clin Oncol 2016;13:77-8.

66. Herbst RS, Soria JC, Kowanetz M, et al. Predictive correlates of response to the anti-PD-L1 antibody MPDL3280A in cancer patients. J Immunol 2014;515:563-7.

67. Homet Moreno B, Zaretsky JM, Garcia-Diaz A, et al. Response to programmed cell death-1 blockade in a murine melanoma syngeneic model requires costimulation, CD4, and CD8 T cells. Cancer Immunol Res 2016.

68. Gao J, Shi LZ, Zhao H, et al. Loss of IFN-gamma Pathway Genes in Tumor Cells as a Mechanism of Resistance to Anti-CTLA-4 Therapy. Cell 2016;167:397-404 e9.

69. Carretero R, Wang E, Rodriguez AI, et al. Regression of melanoma metastases after immunotherapy is associated with activation of antigen presentation and interferon-mediated rejection genes. Int J Cancer 2012;131:387-95.

70. Spranger S, Bao R, Gajewski TF. Melanoma-intrinsic beta-catenin signalling prevents anti-tumour immunity. Nature 2015;523:231-5.

71. Rooney MS, Shukla SA, Wu CJ, Getz G, Hacohen N. Molecular and genetic properties of tumors associated with local immune cytolytic activity. Cell 2015;160:48-61.

72. Inoue H, Park JH, Kiyotani K, et al. Intratumoral expression levels of PD-L1, GZMA, and HLA-A along with oligoclonal T cell expansion associate with response to nivolumab in metastatic melanoma. Oncoimmunology 2016;5:e1204507.